

# Bioresorbable Metals for Biomedical Applications: From Mechanical Components to Electronic Devices

Hanjun Ryu, Min-Ho Seo,\* and John A. Rogers\*

**Bioresorbable metals and metal alloys are of growing interest for myriad uses in temporary biomedical implants. Examples range from structural elements as stents, screws, and scaffolds to electronic components as sensors, electrical stimulators, and programmable fluidics. The associated physical forms span mechanically machined bulk parts to lithographically patterned conductive traces, across a diversity of metals and alloys based on magnesium, zinc, iron, tungsten, and others. The result is a rich set of opportunities in healthcare materials science and engineering. This review article summarizes recent advances in this area, starting with an historical perspective followed by a discussion of materials options, considerations in biocompatibility, and device applications. Highlights are in system level bioresorbable electronic platforms that support functions as diagnostics and therapeutics in the context of specific, temporary clinical needs. A concluding section highlights challenges and emerging research directions.**

transient biological processes such as wound healing.<sup>[6–9]</sup> Mechanisms of biore sorption naturally eliminate a potential source of infection and of other complications, as well as risks and costs associated with secondary surgical procedures for retrieval.<sup>[10–13]</sup> Among various classes of bioresorbable materials, metals are particularly important, historically due to their favorable mechanical properties in structural components.<sup>[14]</sup> Since early reports of joint arthroplasties based on magnesium (Mg) plates and sheets in 1900,<sup>[15–17]</sup> bioresorbable metals have appeared in many different orthopedic applications, from bone fracture fixture screws, to nails, plates and pins from 1909 to 1948<sup>[18–21]</sup> (Figure 1). In other examples, cylindrical mesh structures of Mg and iron (Fe) stents act as temporary vascular stents in balloon angioplasty

procedures and others in 2001.<sup>[22]</sup> Mg and Mg alloys can also serve as scaffolds for tissue regeneration in 2006.<sup>[23]</sup>

Interest in bioresorbable metals now also includes their use as thin film conductors in bioresorbable electronic devices, since 2009.<sup>[24–33]</sup> Here, techniques in microfabrication adapted from those used in the integrated circuit industry allow for precise patterning of these metals into electrodes, interconnects, interlayer

## 1. Introduction

Bioresorbable (or, equivalently, bioabsorbable) organic and inorganic materials serve as the basis for biomedical implants that chemically react in a controlled manner with biofluids to yield soluble and biocompatible end products.<sup>[1–5]</sup> The interest is in devices that serve temporary functions in the body in the context of

Dr. H. Ryu, Prof. J. A. Rogers  
 Center for Bio-Integrated Electronics  
 Querry Simpson Institute for Bioelectronics  
 Northwestern University  
 Evanston, IL 60208, USA  
 E-mail: jrogers@northwestern.edu  
 Prof. M.-H. Seo  
 School of Biomedical Convergence Engineering  
 College of Information & Biomedical Engineering  
 Pusan National University 49  
 Busandaehak-ro Yangsan-si, Gyeongsangnam-do 50612,  
 Republic of Korea  
 E-mail: mhseo@pusan.ac.kr  
 Prof. J. A. Rogers  
 Department of Mechanical Engineering  
 Northwestern University  
 Evanston IL 60208, USA

Prof. J. A. Rogers  
 Department of Civil and Environmental Engineering  
 Northwestern University  
 Evanston IL 60208, USA  
 Prof. J. A. Rogers  
 Department of Materials Science and Engineering  
 Northwestern University  
 Evanston IL 60208, USA  
 Prof. J. A. Rogers  
 Department of Biomedical Engineering  
 Northwestern University  
 Evanston IL 60208, USA  
 Prof. J. A. Rogers  
 Department of Chemistry  
 Northwestern University  
 Evanston IL 60208, USA  
 Prof. J. A. Rogers  
 Department of Electrical and Computer Engineering  
 Northwestern University  
 Evanston IL 60208, USA  
 Prof. J. A. Rogers  
 Departments of Neurological Surgery  
 Feinberg School of Medicine  
 Northwestern University  
 Chicago IL 60611, USA

 The ORCID identification number(s) for the author(s) of this article can be found under <https://doi.org/10.1002/adhm.202002236>

DOI: 10.1002/adhm.202002236

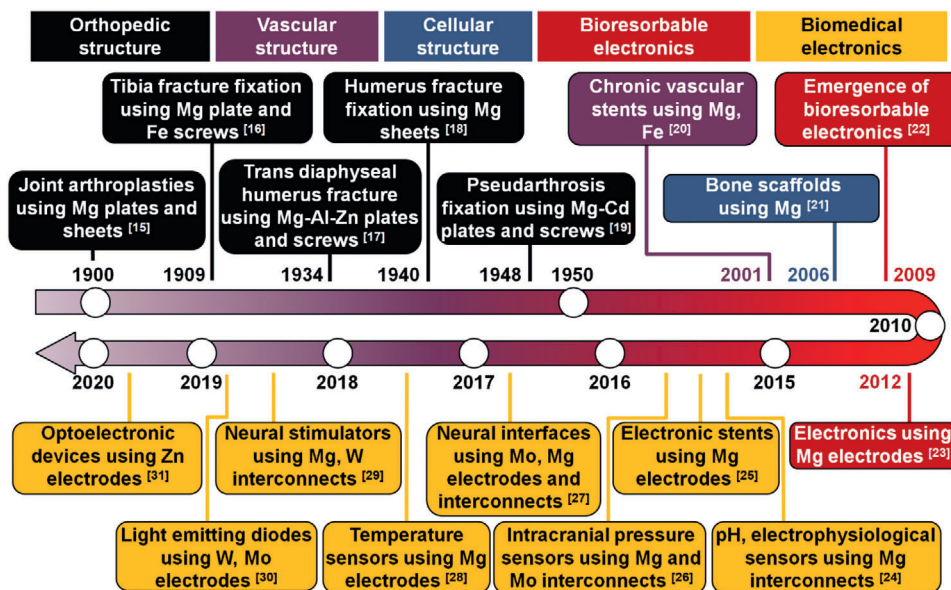


**Figure 1.** Timeline for the development of biomedical applications of bioresorbable metals. The earliest work focused on mechanical applications, such as orthopedic (black), vascular (purple) and cellular (blue) structures. Demonstrations of electronics that use bioresorbable metals are relatively recent (2009 and 2012; red). Recent examples include wireless systems for diagnostic and therapeutic applications (yellow).

vias and other essential elements for electronic devices and systems that often also exploit bioresorbable semiconductors and dielectrics for active functionality.<sup>[34]</sup> Examples range from antennas and transistors, to diodes, inductors, capacitors, and other components that can be integrated into highly sophisticated active implants capable of performing various diagnostic and therapeutic functions that intersect with clinical needs.<sup>[35]</sup>

This review summarizes the materials science of bioresorbable metals in all of these contexts. Discussions include options in materials selections, considerations in biocompatibility and applications in devices, ranging from structural components to electronic systems. The first sections focus on aspects in materials chemistry and biocompatibility. Following content highlights various uses of bioresorbable metals in established implants that provide mechanical function, including bone fixtures, stents, and scaffolds. The topics then shift to the latest research in electronic devices, where the metals appear as vapor-deposited thin films, laser-processed thin foils or metallic composites, and printable inks. The emphasis spans isolated elements to integrated circuits and electronic platforms. Descriptions throughout this review include chemical and biochemical aspects of bioresorption for each case. A concluding section summarizes the current state of the field and highlights opportunities for further research.

## 2. Chemical Processes That Govern Bioresorption of Metals

Bioresorbable metals such as Mg, zinc (Zn), Fe, molybdenum (Mo), and tungsten (W) have well-established roles as temporary orthopedic, vascular implants, and in recent work, as conductors in bioresorbable electronics.<sup>[36–40]</sup> The favorable mechanical properties and biocompatible characteristics of these materials align well with requirements for structural applications. In some cases, bioresorption not only eliminates the need for surgical re-

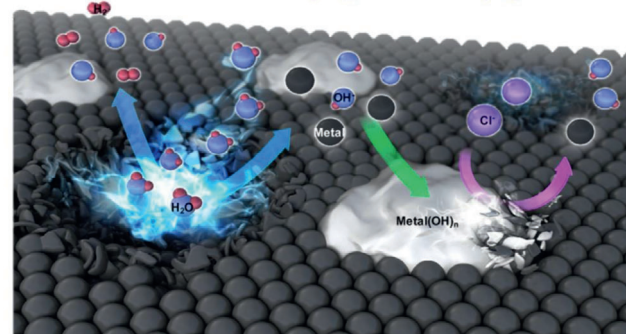
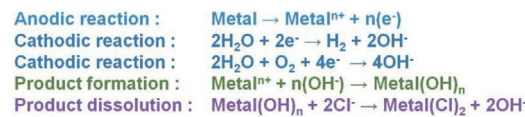


**Figure 2.** Schematic illustration of chemical processes for bioresorption of metals. Reproduced with permission.<sup>[41]</sup> Copyright 2018, Elsevier Ltd.

moval, but it also yields products that enhance the restoration of damaged tissues.<sup>[16,41,42]</sup> Reactions of Mg, Zn, and Fe in biofluids at physiological conditions occurs through a series of anodic and cathodic processes. In general, hydrolysis converts the metals to more stable ions (Figure 2) that then undergo oxidation.<sup>[41]</sup> For metals such as Mg, Zn, and Fe this first step generates metal cations following the anodic reaction (metal → metal<sup>n+</sup> + ne<sup>-</sup>). The generated electrons participate in a cathodic reaction corresponding to water reduction ( $2\text{H}_2\text{O} + 2\text{e}^- \rightarrow \text{H}_2 + 2\text{OH}^-$ ) for Mg and Zn, with corresponding reduction of dissolved oxygen ( $2\text{H}_2\text{O} + \text{O}_2 + 4\text{e}^- \rightarrow 4\text{OH}^-$ ) in the case of Fe. The overall hydrolysis reactions for Mg, Zn, and Fe are  $\text{Mg} + 2\text{H}_2\text{O} \rightarrow \text{Mg}(\text{OH})_2 + \text{H}_2$ ,  $\text{Zn} + 2\text{H}_2\text{O} \rightarrow \text{Zn}(\text{OH})_2 + \text{H}_2$ , and  $4\text{Fe} + 3\text{O}_2 + 10\text{H}_2\text{O} \rightarrow 4\text{Fe}(\text{OH})_4^- + 4\text{H}^+$ , respectively.<sup>[10,43–45]</sup> Mo and W also resorb

through hydrolysis reactions ( $2\text{Mo} + 2\text{H}_2\text{O} + 3\text{O}_2 \rightarrow 2\text{H}_2\text{MoO}_4$ ,  $2\text{W} + 2\text{H}_2\text{O} + 3\text{O}_2 \rightarrow 2\text{H}_2\text{WO}_4$ ),<sup>[10,46,47]</sup> although with rates that can be much lower than those of Mg, Zn, and Fe.<sup>[44]</sup>

As these reactions occur over the surfaces of metal parts or films, galvanic coupling arises due to different potentials between the metal matrix and the intermetallic phase, or the grain boundaries. Simultaneously, organic molecules, such as proteins, amino acids, and lipids, often adsorb onto the surfaces, thereby influencing these reactions. The formation of Metal(OH)<sub>n</sub> on the surface (metal<sup>n+</sup> + nOH<sup>-</sup> → metal(OH)<sub>n</sub>) can depend strongly on additional aspects of the physiological environment, specifically the concentration of chloride ions (Cl<sup>-</sup>). Adsorption of Cl<sup>-</sup> initiates breakdown of the metal(OH)<sub>n</sub> protective layer and leads to pitting corrosion. As the degradation proceeds, calcium phosphate-based apatite in the surrounding biofluids can deposit onto the undissolved metal(OH)<sub>n</sub> due to localized alkalization and to saturation of calcium and phosphate in biofluids. Over time, adhered cells often proliferate to form tissues adjacent to the corrosion product layer. Meanwhile, eroded biodegradable metals may disintegrate from the bulk metal as particles that can migrate into the surrounding media. Such phenomena occur typically with Mg, but relatively rarely with Fe. Depending on their sizes, fibrous tissues or macrophages can enclose these fragments throughout the dissolution period until the metallic phase is completely exhausted.<sup>[48]</sup>

### 3. Biocompatibility of Biodegradable Metals

Extensive studies of the biocompatibility of structural components formed with biodegradable metals can be found in the literature. In most applications, the total masses of the metals are in the range of hundreds of mg for screws to a few mg for scaffolds. By contrast, uses in electronic systems involve comparatively minute amounts, hundreds of µg, or less, for representative devices.<sup>[28,49]</sup> Cytotoxicity (any substance or process that kills cells) and genotoxicity (any substance or process that damages genetic information) are important parameters in assessments of biocompatibility of biodegradable metals. Tests for biodegradable metals follow the International Organization for Standardization (ISO) 10993-5 protocols for in vitro evaluations of cytotoxicity.<sup>[50]</sup> ISO 10993-3 provides protocols for in vitro evaluations of genotoxicity.<sup>[51]</sup> The comet assay is the most common method for assessing genotoxicity, a characteristic that XTT or other cytotoxicity tests cannot capture. The half-maximal inhibitory concentration (IC<sub>50</sub>; the amount of a chemical species needed to inhibit a biological function by half),<sup>[52]</sup> the median lethal concentration (LC<sub>50</sub>; the concentration of a chemical species in a cell culture needed to cause the death of 50% of test cells after a specified time duration),<sup>[53]</sup> and the median lethal dose (LD<sub>50</sub>; a single dose of a chemical species needed to cause the death of 50% of the test subjects)<sup>[54]</sup> represent common metrics for assessments of biocompatibility. Published reports that use extracts of metal powders in Ringer's solution indicate IC<sub>50</sub> values for fibroblast cells (L929) of ≈200 µg mL<sup>-1</sup> for Mo.<sup>[55]</sup> Other studies use metal salts, such as MoCl<sub>5</sub>, WCl<sub>6</sub>, FeCl<sub>3</sub>, and ZnCl<sub>2</sub>, to examine the toxicity of metal ions on tissues and organs using the same cell lines.<sup>[56]</sup> These measurements define IC<sub>50</sub> values for MoCl<sub>5</sub>, WCl<sub>6</sub>, FeCl<sub>3</sub> and ZnCl<sub>2</sub> of 325, 247, 879, and 13 µg mL<sup>-1</sup>, respectively, for L929. Another measure of toxicity, the

LC<sub>50</sub> is 670 µg mL<sup>-1</sup> ( $7 \times 10^{-3}$  M) for Mo<sup>5+</sup> for human osteosarcoma cells (MG63).<sup>[57]</sup> Other investigations examine the potential local toxicity of W on human pulmonary arterial endothelial cells (EC), smooth muscle cells (SMC) and human dermal fibroblasts (FB).<sup>[58]</sup> In vitro cytopathologic experiments using coils of W (corrosion rates (CR), 29 µg per day) reveal that EC exhibit a 50 µg mL<sup>-1</sup> LD<sub>50</sub> for W. The LD<sub>50</sub> of W for SMC and FB are 100 and 1000 µg mL<sup>-1</sup>, respectively, after 10 d of incubation.

Cytotoxicity studies of biodegradable thin films, nanoparticles (NPs), or composites can reveal aspects of biocompatibility for small amounts of biodegradable metals, specifically for uses in electronics. One paper reports the cytotoxicity of films of high purity Mg (99.99%) using L929, MG63, and vascular smooth muscle cells (VSMC, Figure 3a).<sup>[59]</sup> Cell viability (live cells/total cells × 100%; over 80% defines biocompatibility<sup>[50]</sup>) results from LIVE/DEAD cell assays (LIVE/DEAD staining kit, BestBio) indicate that concentrations of ≈63 µg mL<sup>-1</sup>, 632 µg mL<sup>-1</sup>, and <316 µg mL<sup>-1</sup> exhibit no cytotoxicity to L929, MG63, and VSMC, respectively, in the pH range of 7.5–9.0. Additional results indicate no significant cytotoxicity for 200 µg mL<sup>-1</sup> of Mo NPs (maximum up to 800 µg mL<sup>-1</sup>; data not shown) for human breast (MCF-7) and fibrosarcoma (HT-1080) cells (Figure 3b).<sup>[60]</sup> Another study evaluates Fe foil on human umbilical vein endothelial cells (HUVECs) using colorimetric cell viability kits (WST-8). The results indicate toxicity of Fe above 50 µg mL<sup>-1</sup> for HUVECs.<sup>[61]</sup> Other investigations examine the toxicity of foils of Zn on human endothelial cells (HAEC), human aortic smooth muscle cells (AoSMC), and human dermal fibroblasts (hDF).<sup>[62]</sup> The tetrazolium salt assay kit based on 2,3-bis(2-methoxy-4-nitro-5-sulfophenyl)-2H-tetrazolium-5-carboxanilide (XTT) reveals LD<sub>50</sub> values of ≈3.5 µg mL<sup>-1</sup> ( $50 \times 10^{-6}$  M), ≈4.5 µg mL<sup>-1</sup> ( $70 \times 10^{-6}$  M), and ≈17.5 µg mL<sup>-1</sup> ( $265 \times 10^{-6}$  M) for hDF, AoSMC, HAEC, respectively. Additional assays define the effects of W thin films and fully formed electronic microcomponents (device-grade silicon nanomembranes (Si NM), silicon dioxide (SiO<sub>2</sub>), SiN<sub>x</sub>, and W) on the mechanobiology of CCD18 human colon fibroblasts using cell culture media (Dulbecco's modified Eagle medium, fetal bovine serum (10% v/v), and penicillin–streptomycin (1%)).<sup>[34]</sup> These experiments examine traction forces as cells sense the stiffness of the surrounding environment and transduce mechanical information into cellular responses.<sup>[63]</sup> The dissolved components of the materials studied in this work (6.36 µg mL<sup>-1</sup> for Si, and 78.3 µg mL<sup>-1</sup> for W) indicate no significant perturbations in mechanobiological signatures.

In vivo cytotoxicity studies of biodegradable structural components yield information on biocompatibility relevant to clinical use. Investigations of Fe stents (18 mm in diameter × 3 mm in length, 13 mg) in mini-swine models (8–9 month old, 25–35 kg)<sup>[66]</sup> with immunohistochemical staining and vascular histomorphometry reveal negligible differences in responses compared to those of conventional nonbiodegradable stents (cobalt-chromium bare-metal stent; VISION, Abbott Vascular, USA) after 28 d insertion. Blood platelet (PLT) counts, biochemical parameters including red/white blood cells (RBC and WBC), aspartate aminotransferase (AST), alanine aminotransferase (ALT), triglycerides (TG), total cholesterol (TC), and blood urea nitrogen (BUN) all remain in a normal range. Additional studies examine MgF<sub>2</sub> coated Mg and MgF<sub>2</sub> coated MgNdZrZn alloy (JDBM) scaffolds in rats and rabbits (Figure 3c).<sup>[64]</sup> Histological

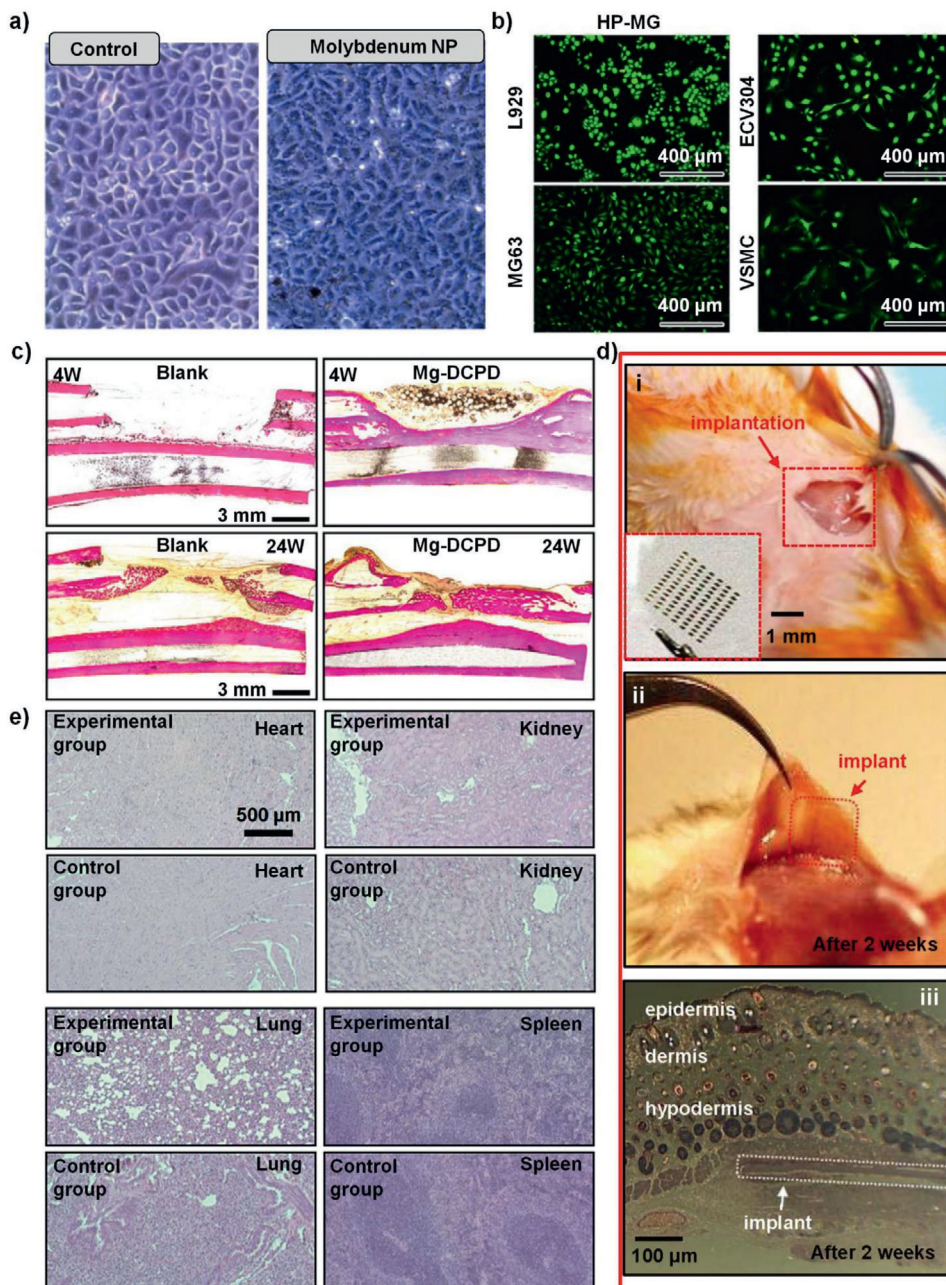


**Figure 3.** Studies of biocompatibility for bioresorbable metals. a) LIVE/DEAD staining of cells after culturing in Mg. Adapted with permission.<sup>[59]</sup> Copyright 2018, American Chemical Society. b) Viability of MCF-7 cells and HT-1080 cells cultured with Mo NPs. Adapted with permission.<sup>[60]</sup> Copyright 2015, Elsevier Inc. c) Van Gieson staining of undecalcified sections; red represents bone tissue and black represents the residual scaffold material. Adapted with permission.<sup>[64]</sup> Copyright 2020, Elsevier Ltd. d) Optical images of the subcutaneous implantation of a representative device in the dorsal region of a BALB/c mouse (i, ii). Image of the implant site after 2 weeks, indicating complete bioresorption (iii). Adapted with permission.<sup>[65]</sup> Copyright 2013, Wiley-VCH GmbH. e) Histological images of the heart, kidney, lung, and spleen of a control mouse and a mouse with a bioresorbable spectrometer 5 weeks after implantation. Adapted with permission.<sup>[33]</sup> Copyright 2019, The Author(s), under exclusive license to Springer Nature Limited.

analysis (Van Gieson's, hematoxylin and eosin (H&E), Masson, and immunohistochemistry stains) confirms that small scaffolds (3 mm in diameter, 5 mm in height) for Sprague Dawley (SD) rats (male, 250 g) and large scaffolds (5 mm in diameter, 15 mm in height) for rabbits (male, 2.5 kg) show no significant signs of toxicity. Other experiments involve cylindrical disks of Zn and

Zn-2Fe alloy (7 mm in diameter, 2 mm in height) inserted into Wistar rats.<sup>[67]</sup> Histological analysis of subcutaneous tissues after 14 weeks of implantation confirms no inflammation. Another publication reports clinical results (63 patients) using commercial Mg stents (10–15 mm in length, 3–3.5 mm in diameter; Biotronik, Germany).<sup>[68]</sup> The data indicate no fatal or non-fatal

cases of myocardial infarction, in-hospital death or acute stent thrombosis.

Recent research includes *in vivo* examinations of the biocompatibility of thin films of bioresorbable metals, as used in electronic applications. One example reports on bioresorbable silicon transistors (doped Si (100 nm in thickness),  $\text{SiO}_2$  gate oxide (100 nm in thickness), and source, drain and gate electrodes of Mg (200 nm in thickness); 13 × 7 arrays; on films of silk fibroin (5 mm × 5 mm × ≈2 µm) sterilized by ethylene oxide and then inserted through incisions on the backs of Balb/c mouse models (see Figure 3d-i) in accordance with institutional IACUC-approved protocols. Visual inspection after 2 weeks of tissues surrounding the implanted sample (see Figure 3d-ii) reveals no signs of remaining Mg or Si. Histological examination indicates an absence of inflammatory responses (see Figure 3d-iii).<sup>[65]</sup> Similar and additional investigations that include hematology and biochemistry studies focus on Zn thin films in bioresorbable devices that include photodetectors (Si NM with dimensions of 500 µm × 500 µm × 1500 nm, and a pair of Zn electrodes with dimensions of 2000 µm × 250 µm × 400 nm) and an optical fiber (poly(lactic-co-glycolic acid) (PLGA) with a diameter of 150 µm) using similar mouse models and procedures. The measurements include concentrations of Zn in the blood, brain, heart, kidney, liver, lung, muscle, and spleen tissues assessed from explantation at 1, 3, 5, and 7 weeks after device implantation. The results in all cases indicate no abnormal accumulation of dissolved Zn in these tissues during the 7 week implantation period. Elevated concentrations of Zn that appear during the first 3 weeks of study in some tissues gradually return to the normal range within 7 weeks. Furthermore, computed tomography (resolution: ≈30 µm<sup>3</sup>) images reveal no signs of Zn after 41 d. Histological analysis of key organ tissues (heart, kidney, lung, and spleen) shows no damage to or identifiable immune cells related to implantation (Figure 3e).<sup>[33]</sup>

Additional studies examine printable conductors formed using composites of bioresorbable metal particles in organic matrices. In one example, subcutaneous implantation of a 1 cm × 1 cm × 800 µm piece of W microparticles embedded in candelilla wax (conductive (C)-wax) in the abdominal region of mouse models lead to no changes in gross histology or immune cell infiltration, as defined by tissue sections stained with H&E.<sup>[69]</sup> Further quantified evaluations of immune reactions that use staining of the CD45 antibodies, a pan-immune cell marker, also show no anomalies. Similar lack of differences appears in data on weight gain, consistent with no observable effect on the overall animal health and patterns of growth.

## 4. Bioresorbable Metals for Structural Applications

### 4.1. Bioresorbable Fixtures

Biodegradable polymers can offer mechanical properties similar to those of targeted tissues, they can be molded and formed into diverse shapes easily, and they can present platforms for robust cell attachment, as promising candidates for organ regeneration.<sup>[70]</sup> Resorbable sutures are likely the most widely used class of device enabled by bioresorbable polymers, again due to their mechanical flexibility and ease of processability.<sup>[71]</sup> Such materials can also be doped with various types of drugs to support controlled release, with many examples of important

applications.<sup>[72]</sup> By comparison to polymers, metals are attractive for structural applications because of their favorable impact strength, wear resistance, ductility, and toughness. One such application is in fixtures based on plates and screws that hold a fractured bone together.<sup>[73]</sup> High ductility in such cases can be useful due to the common need to bend a fixture during a surgical procedure. Low CRs can help to prevent adverse side effects on the healing process. Specifically, the requirements are for CR less than 0.5 mm per year in simulated body fluids at 37 °C, strengths higher than 200 MPa, and levels of elongation greater than 10%.<sup>[74]</sup> Bioresorbable metals such as Mg alloys are attractive candidates because they offer such properties, along with densities that are lower than those of other metal options.<sup>[75]</sup> Such alloys must combine high strength with relatively low modulus (tens of GPa), close to that of bone (3–20 GPa), to avoid effects known as stress shielding.<sup>[76]</sup> Here, an implantable structure that has a stiffness (e.g., stainless steels: ≈200 GPa, Cr-Co alloys: ≈230 GPa, Ti alloys: ≈115 GPa) much higher than that of human bone can carry most of the load, thereby leading to decreases in bone mass, over time. Stress concentrations around the implant structure can also cause bone refracture after removal of the structure.<sup>[77–80]</sup> Appropriately designed bioresorbable metals can meet these demanding requirements for orthopedic load-bearing and fixation structures, with uses in joint replacement, bone plates, screws, dental implants, and coronary stents.<sup>[81,82]</sup>

The processes of bioresorption alter the shapes, morphologies, and sectional areas of the constituent parts in ways that change their mechanical properties and load-bearing characteristics. As an example, experiments define the changes in the tensile strength of Mg alloys (ZX11; Mg-0.7Zn-0.6Ca, 1.8 mm in thickness) formed by rolling and annealing processes as a function of time of immersion in modified Eagle medium alpha ( $\alpha$ -MEM + 10% fetal bovine serum (FBS)) under cell culture conditions (37 °C, 5% CO<sub>2</sub>, 20% O<sub>2</sub>, 95% relative humidity, see Figure 4a).<sup>[83]</sup> In both rolled and annealed ZX11 samples, the mechanical strength decreases over several weeks, by magnitudes that are consistent with calculation results based on the reduced cross-sectional areas. At subsequent stages, the strength diminishes at rates faster than expected, likely due to pitting, nonuniform degradation, and resulting local defects that act as stress risers and locations of catastrophic failure. Additionally, localized degradation can promote the diffusion of hydrogen into the material, resulting in embrittlement.<sup>[84]</sup>

The desired timescales for use are important considerations in the selection of materials and structure geometries. For instance, reunion of bone fractures occurs over 12–18 weeks. Various alloys of Mg are suitable, including, ZEK 100 (MgZnZrRE),<sup>[87]</sup> LAE 442 (Mg-4Li-4Al-2RE),<sup>[88]</sup> Mg-0.8Ca,<sup>[89]</sup> and MgYREZr,<sup>[90]</sup> as demonstrated in bone screws for animal models and human clinical trials. Studies in animals over 12 months confirm that these materials also have osteogenic effects, without adverse consequences of hydrogen evolution. Comparison results show that Mg-0.8Ca yields stronger bone-implant contacts than LAE442. Also, Mg-0.8Ca screws exhibit good tolerability, as a measure of the degree to which adverse effects can be tolerated by the subject. These components also show excellent biomechanical properties, comparable to those of 316L stainless steel screws in the first 2–3 weeks after implantation in adult rabbits. Other investigations reveal that MgYREZr alloy is clinically equivalent to Ti for screws

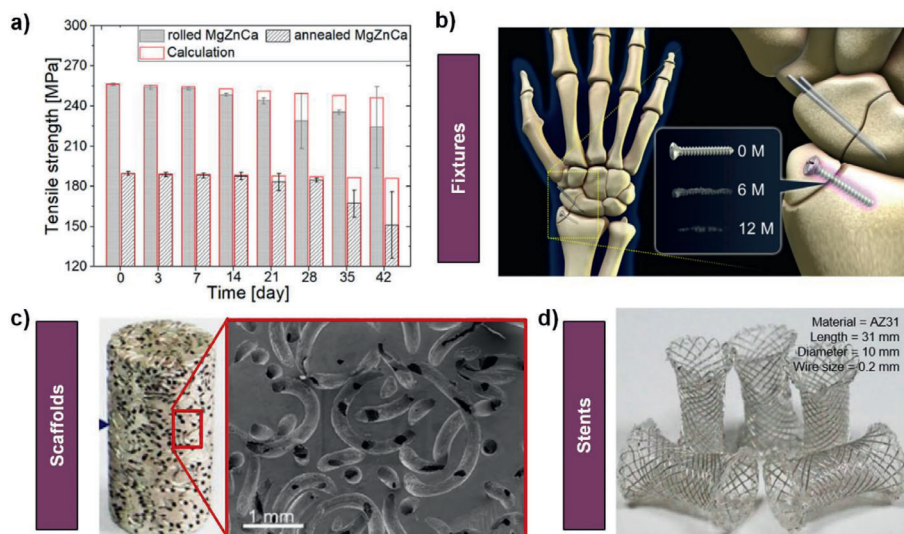


**Figure 4.** Uses of bioresorbable metals in structural applications. a) Changes in ultimate tensile stress of rolled and annealed ZX11 alloy (MgZnCa) after different times of immersion in  $\alpha$ -MEM with 10% FBS under cell culture conditions ( $37\text{ }^{\circ}\text{C}$ , 5%  $\text{CO}_2$ , 20%  $\text{O}_2$ , 95% rel. humidity). The calculation results capture decreases in strength caused by reductions in the sectional area associated with bioresorption. Adapted with permission.<sup>[83]</sup> Copyright 2019, Acta Materialia Inc. b) Representative structural application of bioresorbable metals; Mg-5Ca-1Zn alloy as screws for treating distal radius fracture. Adapted with permission.<sup>[73]</sup> Copyright 2016, National Academy of Sciences. c) Porous Mg scaffolds for tissue engineering. Adapted with permission under the terms of the creative commons license.<sup>[85]</sup> Copyright 2016, The Author(s). Published by Springer Nature. d) Mg-Zn alloy AZ31 in esophageal stents. Adapted with permission under the terms of the creative commons license.<sup>[86]</sup> Copyright 2018, The Author(s). Published by SAGE Publishers.

used in the treatment of mild hallux valgus deformities.<sup>[90]</sup> Recent long-term clinical studies yield information on the performance of Mg-5Ca-1Zn alloy screws in 53 distal radius fracture fixation cases.<sup>[91]</sup> Longitudinal investigations indicate that the diameters of the Mg alloy screws decrease significantly after 6 months. After complete healing of the fracture at 12 months, the remaining material cannot be distinguished by X-ray imaging from new surrounding bones (Figure 4b).<sup>[73]</sup>

#### 4.2. Bioresorbable Scaffolds

Scaffolds, designed as 3D porous solid frameworks capable of providing structural support for cell attachment and tissue regeneration, represent another type of structural application. The porosity and bioactivity of these systems can promote cell proliferation and differentiation.<sup>[92,93]</sup> The mechanical properties can bear forces that occur at the scaffold-tissue interface during healing or generation of neotissues, without fracture or collapse. The biodegradability of the constituent materials allows for replacement by biological tissues via physiological extracellular components without leaving residues or toxic degradation products. The inherent strength and ductility of biodegradable metals represent key attractive features in this context.<sup>[94,95]</sup> Research demonstrates the applicability of Mg and Fe, and various alloys of these metals, for bone replacement scaffolds for cases of pure Mg, Mg-RE (rare earth elements), Mg-Ca, pure Fe, Fe-Mn alloys, and Fe foams (Figure 4c).<sup>[85]</sup> The minimum recommended pore size is 100  $\mu\text{m}$  and the porosity should exceed 50%. These considerations must be balanced by those associated with mechanical requirements. Mg and its alloys can satisfy these needs for porous scaffolds as orthopedic implants, and the densities are close to

those of natural bones ( $1.8\text{--}2\text{ g cm}^{-3}$ ). One fabrication process exploits infiltration of molten Mg into 3D entanglements of Ti wires, as a sacrificial material that can be removed by chemical etching. Mg scaffolds of this type have a CR of  $\approx 1.5\text{ mm per year}$ , at a porosity of  $\approx 54\%$ , a pore size of  $400\text{ }\mu\text{m}$ , and offer a comprehensive strength of  $\approx 46\text{ MPa}$ , and Young's modulus of  $\approx 2.23\text{ GPa}$ . Live/dead staining, subcutaneous/intramuscular inflammatory response evaluations, together with internal organ histology, histological, and immunohistological analysis demonstrate that Mg scaffolds are biocompatible, with complete degradation at 16 weeks after implantation.

Recently developed Zn scaffolds provide another option, with rates of bioresorption similar to those of tissue regeneration, with acceptable cytocompatibility, and with antibacterial properties.<sup>[96-98]</sup> One example involves a Zn scaffold (13 mm in diameter and 11 mm in height) with a perimeter of  $\approx 7\text{ mm}$ , a porosity of 60%, a Young's modulus of  $\approx 100\text{ MPa}$ , a yield strength of  $\approx 6\text{ MPa}$ , and a CR of  $\approx 145\text{ }\mu\text{m per year}$  in modified Hank's solution at  $37\text{ }^{\circ}\text{C}$ . Studies based on cell adhesion and the 3-(4,5-dimethylthiazol-2-yl)-2,5-diphenyl tetrazolium bromide (MTT) assay confirm acceptable levels of biocompatibility. Zn scaffolds also provide antibacterial rates that approach  $\approx 100\%$ ,<sup>[97]</sup> thereby resolving a common problem of colonization of bacterial after implantation.<sup>[99]</sup> Biofilms including bacterial colonies, layers of proteins, and collections of cells do not typically form on these types of scaffolds.

#### 4.3. Bioresorbable Stents

Stents represent another application of bioresorbable metals where mechanical characteristics play an essential role.<sup>[100]</sup>

Stents are small mesh structures in cylindrical geometries that serve as supports to prevent recoil of arterial vessels following balloon angioplasty procedures, to open blocked areas of the esophagus, and to maintain passageways that carry bile to digestive organs, that pass air in and out of the lungs, or that carry urine from the kidneys to the bladder.<sup>[100–104]</sup> Certain stents include drug-eluting coatings to prevent the growth of scar tissues.<sup>[105]</sup> Bioresorbable stents are of interest in cases where only temporary support is necessary, such as when remodeling of the arterial wall reinforces its mechanics to prevent subsequent collapse.<sup>[82]</sup> Here, elimination of the stent after the healing process reduces the potential for long-term clinical problems that can originate from conventional permanent stent technologies, such as in-stent restenosis and late stent thrombosis, without the need for prolonged antiplatelet therapy. Bioresorbable stents, like other applications discussed in this section, must balance degradation kinetics with mechanical integrity. Specifically, the devices must maintain sufficient strength over timescales for 6–12 months, as the period expected for vessel remodeling and healing processes.<sup>[82,106–109]</sup> Thereafter, the mechanical integrity can decrease as the degradation progresses, with rates that avoid excessive accumulation of products of this degradation around the implantation site.

Mg is an attractive option, although in its pure form the rates of degradation are higher than those required for stents (Figure 4d).<sup>[86]</sup> The incorporation of Al, Mn, Si, and rare earth elements as alloys can decrease these rates significantly. Specifically, AZ21 (Mg-2Al-1Zn), AZ31 (Mg-3Al-1Zn), WE43 (MgYREZr), AM60B-F (Mg-6Al), ZW21 (MgZnYZr), and WZ21 (MgYZn) Mg alloys show promise.<sup>[91]</sup> For example, commercial stents based on Mg alloys (Magmaris, Biotronik, Germany) demonstrate stable recoil (i.e., ability of the stent to maintain its initial expanded diameter) after 1 h, offer high radial strength (i.e., ability to maintain its diameter) under physiological pressures (from 0 to 80 kPa), and support required times for bioresorption (95% of Mg resorbed at 12 months).

Fe is another interesting candidate for this application<sup>[110]</sup> because its high radial strength and elastic modulus allow for use in stents that have thin structural features. Moreover, the high ductility of Fe provides mechanical stability during implantation. Tests in animal models show promise not only for pure Fe but also for various Fe alloys, the latter of which offer flexibility in choices of mechanical properties and rates of bioresorption. As examples, Fe-35Mn, Fe-10Mn-1Pd, Fe-30Mn-6Si and other alloys that exploit different elements (Mn, Co, Al, W, Sn, B, C, and S) offer high yield strength, tensile strength, elongation, and relevant rates of degradation<sup>[82]</sup>. Compared to Mg, Fe-based stents (IBS, Lifetech Scientific, China) exhibit higher radial strength and larger CR (> 12 months)<sup>[111]</sup> but with a brown coloration that can appear in adjacent tissues due to presence of Fe salts.<sup>[110]</sup>

## 5. Bioresorbable Metals for Electronic Applications

### 5.1. Bioresorbable Electronic Materials and Thin Films

Recent advances in electronic materials and fabrication techniques serve as the foundations for using bioresorbable metals in classes of electronic, optoelectronic, photonic, and microelectromechanical systems that are completely

bioresorbable.<sup>[23–26,28,29,33,112]</sup> The most attractive semiconductor materials are various forms of silicon, where the process of bioresorption involves  $\text{Si} + 4\text{H}_2\text{O} \rightarrow \text{Si(OH)}_4 + 2\text{H}_2$ .<sup>[65]</sup> Thin-film dielectrics can be formed with materials such as  $\text{SiO}_2$ ,  $\text{MgO}$ , and  $\text{Si}_3\text{N}_4$ , with corresponding reactions of  $\text{SiO}_2 + \text{H}_2\text{O} \rightarrow \text{Si(OH)}_4$ ,  $\text{MgO} + \text{H}_2\text{O} \rightarrow \text{Mg(OH)}_2$ , and  $\text{Si}_3\text{N}_4 + 6\text{H}_2\text{O} \rightarrow 3\text{SiO}_2 + 4\text{NH}_3$ .<sup>[10,113]</sup> Thin metal conductors (Mg, Mo, Zn, Fe, and W) paired with these materials can yield nearly all of the essential components of advanced electronic systems based on high-performance complementary metal-oxide-semiconductor (CMOS) circuits that incorporate n-p-channel metal-oxide field-effect transistors (MOSFETs). Many of the bioresorbable metals originally developed for structural applications, as described in previous sections, but others as well, can be used in this context, as thin coatings formed by modern methods in physical and chemical vapor deposition. Such thin metal films can be patterned into interconnection traces, electrode interfaces, conductive pads, inductors and other features, where electrical, rather than mechanical, properties are important.<sup>[25]</sup> The physical (morphological) and electrical degradation characteristics of these thin films are important for their use in electronic systems. The materials science of these processes can be qualitatively distinct in thin films compared to bulk samples. Associated changes in the shapes of patterned traces and their thicknesses are also important to understand, particularly in terms of their effects on electrical properties.

Recent studies describe bioresorbable characteristics of thin films of Mg, Mg-3Al-1Zn alloy (AZ31B), Zn, Fe, Mo, and W, each patterned into serpentine traces with similar widths and lengths (250  $\mu\text{m}$  in width, 50 mm in length), but different thicknesses (Mg, AZ31B, Zn, and Fe with 300 nm thick, Mo with 40 nm thick, and W with 150 nm thick).<sup>[44]</sup> The electrical dissolution rates (EDRs) correspond to conversions of the electrical resistance into an effective (nonphysical) thickness  $h$ , according to  $R = R_0 h_0/h$  where  $R_0$  and  $h_0$  are the initial electric resistance and thickness, respectively. Figure 5a shows some representative measurements of morphological and electrical change, along with values of CR for Mg, AZ31B, Zn, Mo, and W. These results can be understood in terms of both localized defects and grain sizes. Specifically, the resistances of thin films are highly sensitive to nonuniformities in corrosion, especially in patterned traces where defects can lead to electrical opens and infinite resistances by local corrosion. As a result, the EDR is generally significantly higher (over 10 times) than the CR, as for Mg, AZ31B, and Zn. On the other hand, Mo and W exhibit relatively uniform surface corrosion processes and have EDRs lower than those of Mg, AZ31B, and Zn. The slow rate of degradation of surface oxidation layers ( $\text{MoO}_x$  and  $\text{WO}_x$ ) in water (0.2–0.5 nm per day) results in values of EDR for both Mo and W that are only two to three times higher than their corresponding CR.

Figure 5b-e shows examples of Mg (Figure 5b),<sup>[25]</sup> Zn (Figure 5c),<sup>[33]</sup> Mo (Figure 5d),<sup>[29]</sup> and W (Figure 5e).<sup>[112]</sup> The high conductivities of these metals ( $\sigma_{\text{Mg}} = 2.15 \times 10^7 \text{ S m}^{-1}$ ,  $\sigma_{\text{Zn}} = 1.68 \times 10^7 \text{ S m}^{-1}$ ,  $\sigma_{\text{Mo}} = 1.91 \times 10^7 \text{ S m}^{-1}$ , and  $\sigma_{\text{W}} = 1.79 \times 10^7 \text{ S m}^{-1}$ ) are suitable for most applications in electronics, even in films with thicknesses of just a few hundred nanometers. Well-established methods in semiconductor processing, transfer printing, and laser cutting allow rapid patterning of these materials into relevant geometries on various hard and soft

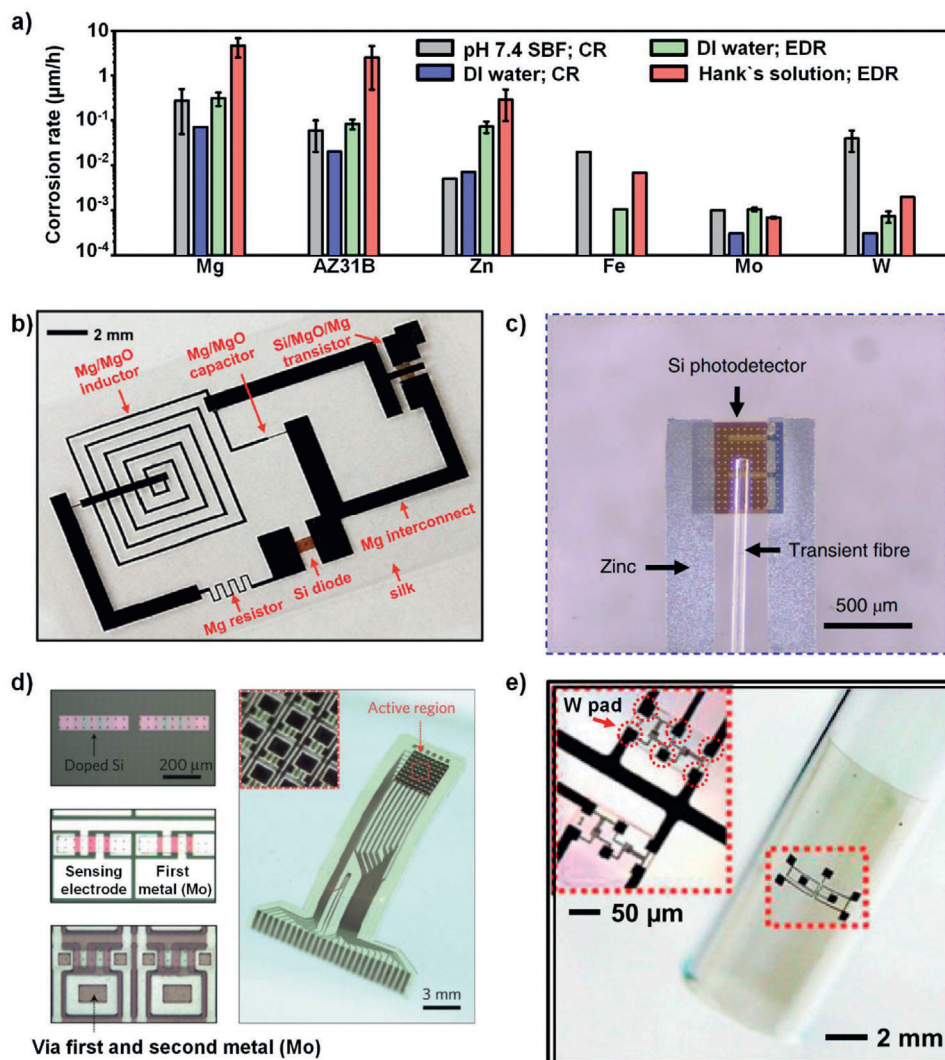


**Figure 5.** Uses of bioresorbable metals as electrodes and electrical interconnects in bioresorbable electronic systems. a) Morphological and electrical measurements of the rates of dissolution of bioresorbable metals in different aqueous solutions. Reproduced with permission.<sup>[44]</sup> Copyright 2013 Wiley-VCH GmbH. b) Optical image of bioresorbable transistors, diodes, inductors, capacitors, and resistors on a silk substrate. Adapted with permission.<sup>[25]</sup> Copyright 2012, American Association for the Advancement of Science (AAAS). c) Optical micrograph of a bioresorbable spectrometer based on thin film Zn electrodes (3 µm-thick). Adapted with permission.<sup>[33]</sup> Copyright 2019, The Author(s), under exclusive license to Springer Nature Limited. d) Optical micrographs of a pair of unit cells at various stages of fabrication (left) and a picture of a complete bioresorbable multiplexed neural electrode array. A patterned thin film of Mo (~300 nm in thickness) serves as the electrode. Adapted with permission.<sup>[29]</sup> Copyright 2016, Nature Publishing Group. e) Optical micrographs of bioresorbable logic gates on a thin film of PLGA wrapped onto a glass cylinder. (Inset: magnified view of the interconnected MOSFETs). All electrodes use thin films of W (~300 nm thick). Adapted with permission.<sup>[112]</sup> Copyright 2017, National Academy of Sciences.

substrates, for use in conventional rigid, planar electronics as well as emerging flexible and stretchable devices.<sup>[33,114]</sup> Initial work in bioresorbable electronics used Mg (150 nm in thickness) for electrodes, interconnects, inductors, capacitors, resistors, diodes, and transistors (see Figure 5b).<sup>[25]</sup> In these systems, Si NMs (70 nm in thickness) served as the semiconductor, with MgO (10 nm in thickness; bioresorbable) and Ti (5 nm in thickness; nonbioresorbable) as dielectrics and adhesion promoters for bonding to thin substrates of silk fibroin. Other studies report bioresorbable optoelectronic devices based on Zn traces and electrodes (400 nm in thickness) with Si photodetectors (1.5 µm in thickness) that interface to PLGA optical fibers (diameter in 150

µm) on PLGA substrates (10 µm in thickness) (see Figure 5c).<sup>[33]</sup> Studies of blood chemistry and hematology results in mouse models implanted with such devices reveal no measurable toxic effects or immune responses in the heart, kidney, lung, or spleen. For long-term stability, Mo is attractive relative to Mg due to its relatively low CR, as demonstrated in source, drain, gate electrodes, and sensing electrode pads (300 nm in thickness) in 64-channel active electronic systems for mapping electrophysiology on the left hemisphere of an anesthetized rat for up to 32 d (see Figure 5d).<sup>[29]</sup> Bioresorbable CMOS devices that use W for vias, electrodes, and interconnects (see Figure 5e)<sup>[112]</sup> are compatible with processes in foundry fabrication of integrated circuits. Here,

W layers with 300 nm thicknesses (and Ti/TiN adhesion layers with 100 nm thicknesses) interconnect MOSFETs to yield CMOS logic gates, such as NAND and NOR circuits.

## 5.2. Bioresorbable Metallic Inks and Composites

Although thin deposited metal films have critical roles in electronics, thick films are often necessary as nonplanar interconnects, low-loss electrical components, solder joints as well as various other features in printed circuit board technologies. Composites of micro/nanoparticles of bioresorbable metals with biodegradable polymers provide important options in conductors that can be patterned by screen printing and related methods. Here, contact between the particles forms percolation pathways for current transport.<sup>[115–117]</sup> Many bioresorbable metals form surface oxides that frustrate these contacts, and their melting temperatures are, in most cases, much higher than the degradation temperatures of polymers used in printable composites. Zn is an exception because microparticles can be sintered using electrochemical means. A recent report describes the development of an ink composed of Zn microparticles (<10 µm) in polyvinylpyrrolidone (PVP) dissolved in isopropyl alcohol (IPA) = 30:1:10 by weight and mixed with an aqueous solution of acetic acid ( $H_2O:CH_3COOH = 10:1$ ).<sup>[115]</sup> Sintering occurs as the acid solution dissolves the layer of ZnO on the microparticles and leads to subsequent self-exchange of Zn and Zn<sup>2+</sup> at the Zn/H<sub>2</sub>O interface. Deposition of Zn from Zn<sup>2+</sup> can form electrical conductive contacts between adjacent particles of Zn, as a type of sintering process. SEM images confirm the formation of these bridges (Figure 6a). The result is a percolating, conductive network within the surrounding polymer matrix, with an increase in conductivity of eight orders of magnitude relative to the unsintered case (see Figure 6b). As an application example, the Zn ink can be used to form radio frequency (RF) antennas on substrates of PLGA (poly(lactic-co-glycolic acid); Figure 6c) for electrical power harvesting.

Patterns of these Zn inks exhibit EDR of <10<sup>4</sup> S m<sup>-1</sup> per day in ambient air. In a desiccator with anhydrous calcium sulfate, the conductivity remains unchanged over a period of 3 weeks. Replacing the hydrophilic polymer matrix with a hydrophobic material can enhance the stability, particularly for systems that use Mo microparticles in place of the Zn (Figure 6d).<sup>[116]</sup> The standard reduction potential ( $V_{SHE}$ ) of Mo is less negative (-0.2 V Mo<sup>3+</sup>/Mo), compared to Zn (-0.76 V Zn<sup>2+</sup>/Zn) and Fe (-0.44 V Fe<sup>2+</sup>/Fe),<sup>[115]</sup> and therefore resists the formation of thick oxides. One composite formulation uses a matrix of poly butanedithiol 1,3,5-trialy-1,3,5-triazine-2,4,6(1H,3H,5H)-trione pentenoic anhydride (PBTPA), first initiated by ultraviolet (UV), and mixed with Mo microparticles (diameters of 1–5 µm). Thermal curing at 250 °C for ≈20 min completes the crosslinking process at temperatures much lower than the oxidation temperature for Mo (700 °C).<sup>[118]</sup> After curing, Mo composites at sufficient loading show good electrical conductivity with prolonged stability compared to otherwise similar composites with hydrophilic polymers such as PLGA. Specifically, at a 0.35 volume fraction of Mo/PBTPA, the DC conductivity is >1000 S m<sup>-1</sup> (Figure 6e). For similar particle sizes, Mo and W (≈10 µm in diameter) yield comparable conductivities due to the similar surface oxidation layers. Calculations

suggest that microparticles with diameters of ≈2 µm provide optimal conductivity, as a balance between volumetric fraction and contacting interface areas. Similar studies of composites based on Zn and Fe microparticles (nonsintered) in PBTPA show conductivities lower than that of Mo (1–5 µm in diameter), mainly due to the formation of nonconductive surface oxide layers and lower intrinsic conductivities. Moreover, this formulation has a viscosity ≈270 Pa s at a shear rate of 0.1 s<sup>-1</sup>, suitable for use with screen printers and other forms of ink writing. Patterns of electrodes and electrical traces with widths between 100 µm and 3 mm, and with thicknesses of 100 µm or more are readily possible, for use in simple demonstrated devices as shown in Figure 6f.

Natural wax materials provide further advantages in hydrophobicity, water permeability, and rate of degradation relative to PBTPA, as demonstrated in recent work that uses W microparticles (≈5 µm diameters) dispersed in candelilla wax (Figure 6g).<sup>[117]</sup> As expected due to percolation effects, the conductivity of the composite increases with the volume fraction of W, to reach a conductivity of >4000 S m<sup>-1</sup> at ≈35 vol% of W/wax (Figure 6h). The resistance is unchanged in ambient conditions for more than 5 d, significantly longer than that achieved with PBTPA. Also, the resistance remains stable up to temperatures of 45 °C, suggesting reliable operation under physiological conditions (37 °C). Processing occurs simply by melting the wax at ≈75 °C followed by solidification, to allow molding, casting, or printing of interconnects, electrodes, bonding pads, and other features with good resolution and dimensional control, using screen printing or writing with a heated metal tip (Figure 6i). Indeed, various bioresorbable electronic devices and interconnections, such as RF antennas and near field communication (NFC) devices, can be achieved easily.

## 6. Bioresorbable Electronic Systems

Recent papers demonstrate the ability to use bioresorbable metal thin films as components of implantable devices with operational characteristics that meet realistic clinical requirements. Here, combining these films with semiconductors, insulators, and encapsulants on supporting substrates can support a range of functions in sensing, switching, data storage, wireless communication, power supply, and energy storage.<sup>[27,28,31,49,119–121]</sup> In some cases, active control and operation after implantation serve both diagnostic and therapeutic purposes.

An early example that addresses a specific clinical need focuses on monitoring intracranial pressure (ICP) and temperature (ICT) during recovery following a severe traumatic brain injury.<sup>[28]</sup> Here, a membrane of PLGA (30 µm in thickness) with a Si NM piezoresistive strain gauge (200 nm in thickness) attaches to a supporting substrate of nanoporous Si (60–80 µm in thickness; 71% porosity) with an etched recess in a manner that allows the membrane to deform by exposure to pressure associated with a surrounding liquid environment (the total size of 1 mm × 2 mm × 0.08 mm<sup>3</sup>, the total weight of ≈0.4 mg) (Figure 7a). The extent of deformation recorded by the strain gauge can be converted to pressure via mechanical modeling and calibration. A thin layer of SiO<sub>2</sub> (100 nm in thickness) electrically passivates the system and provides a barrier against biofluids. Data demonstrate stable operational lifetimes of roughly 3 d. A fine wire of Mo serves as an interconnection between a sensor in

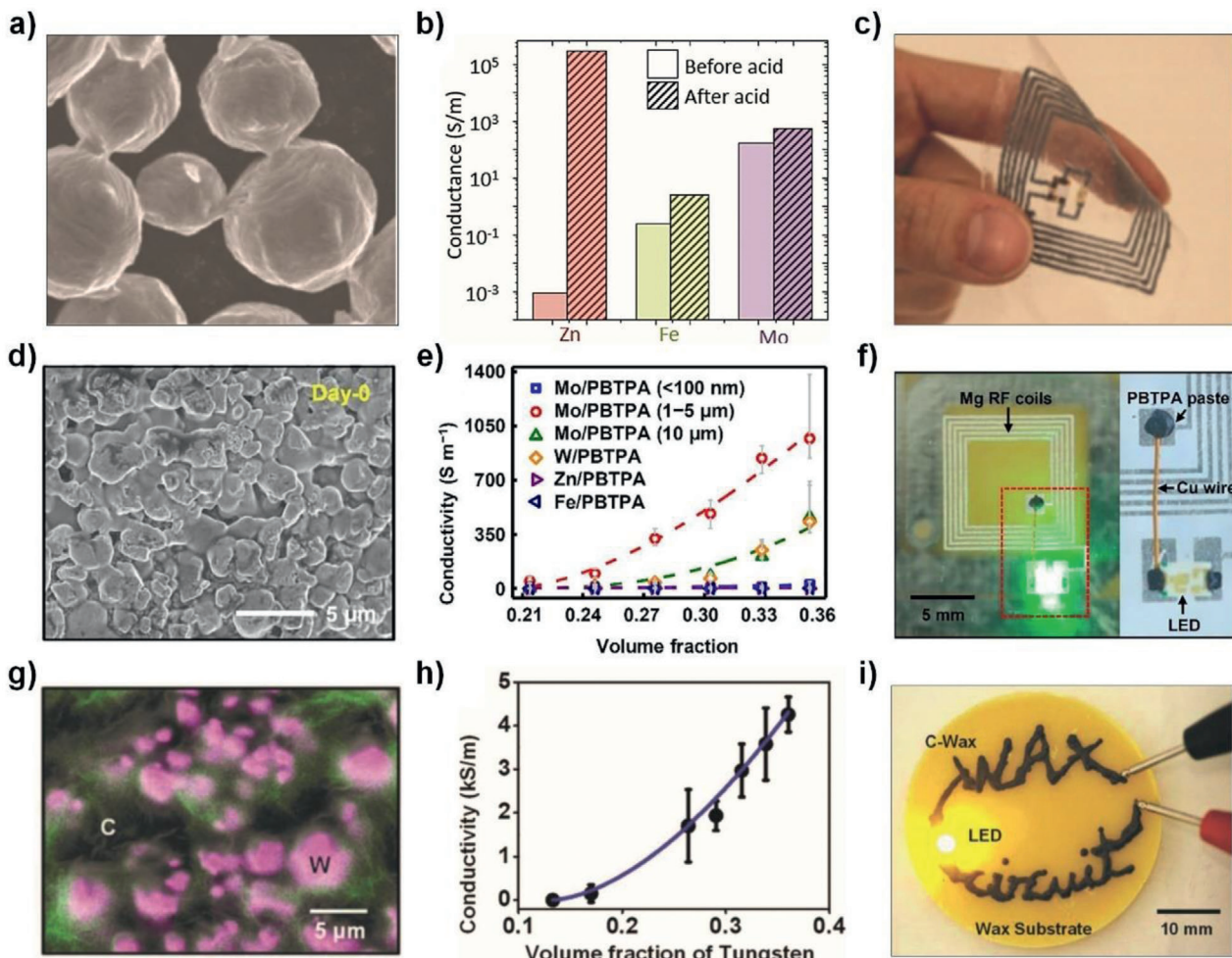


**Figure 6.** Bioresorbable inks as printable conductors and composites. a) SEM image of Zn microparticles sintered at room temperature. b) Conductivities of inks based on microparticles of Zn, Fe, and Mo in matrices of PVP before and after treatment with  $\text{CH}_3\text{COOH}/\text{H}_2\text{O}$ . c) Optical image of near-field communication (NFC) devices with antenna coils (trace widths, 800  $\mu\text{m}$ ) formed by screen-printing of Zn inks on a PLGA substrate. Adapted with permission.<sup>[115]</sup> Copyright 2017, Wiley-VCH GmbH. d) SEM image of a Mo/PBTPA (1:4) metallic composite. e) The conductivity of a composite of microparticles of Mo in PBTPA used as an interconnect between a light emitting diode (LED) and an RF coil of Mg. Adapted with permission.<sup>[116]</sup> Copyright 2018, Elsevier Ltd. g) Colorized SEM image of candelilla wax mixed with W microparticles (C-wax). The green and pink regions correspond to high concentrations of C and W, respectively, determined by energy dispersive spectroscopy (EDS). h) Conductivity of C-wax as a function of volume fraction of tungsten. i) Electrically conductive trace formed by direct writing of C-wax with a heated metal tip, to close a simple circuit through an LED. Adapted with permission.<sup>[117]</sup> Copyright 2018, Wiley-VCH GmbH.

the intracranial space and a subdermal wireless module for data transmission. A version of this device that uses similar operating principles but with significantly increased lifetime and reduced size (Figure 7b) achieves measurement accuracy and precision that compare favorably to those of the most sophisticated clinical standards over periods of up to 25 d, well beyond the typical timeframe of need.<sup>[119]</sup> Key design features include layers of thermally grown  $\text{SiO}_2$  that encapsulate the sensor, structural components that dissolve in a manner that does not affect the measurement accuracy, and durable bonding techniques that prevent water penetration. Sputter-deposited thin films of Mo (100 nm in thickness) as interconnects help to ensure long-term stability.

Other reports describe bioresorbable, wireless pressure sensors for arterial-pulse monitoring.<sup>[120]</sup> The measurement in this

case relies on an LC oscillator that can be probed wirelessly by inductive coupling. A foil of Mg (50  $\mu\text{m}$  in thickness) forms the conducting elements of the capacitor and inductor. The device (5 mm  $\times$  20 mm for the capacitor; 10 mm  $\times$  10 mm for the inductor) consists of two major parts; 1) A fringing-field capacitive sensor that is sensitive to contact with the artery; 2) A bilayer coil inductor that does not contact with the artery. The sensor part wraps the artery such that pulsatile motions lead to deformations in pyramidal microstructures formed on the surfaces of a layer of poly(glycerol sebacate) (PGS, 40  $\mu\text{m}$  in thickness) that serves as the dielectric of the capacitor. These changes lead to shifts in the resonance frequency of the LC oscillator. By folding a pair of inductor coils into an overlapping configuration, frequencies in the hundreds of MHz range can be realized, where absorption by

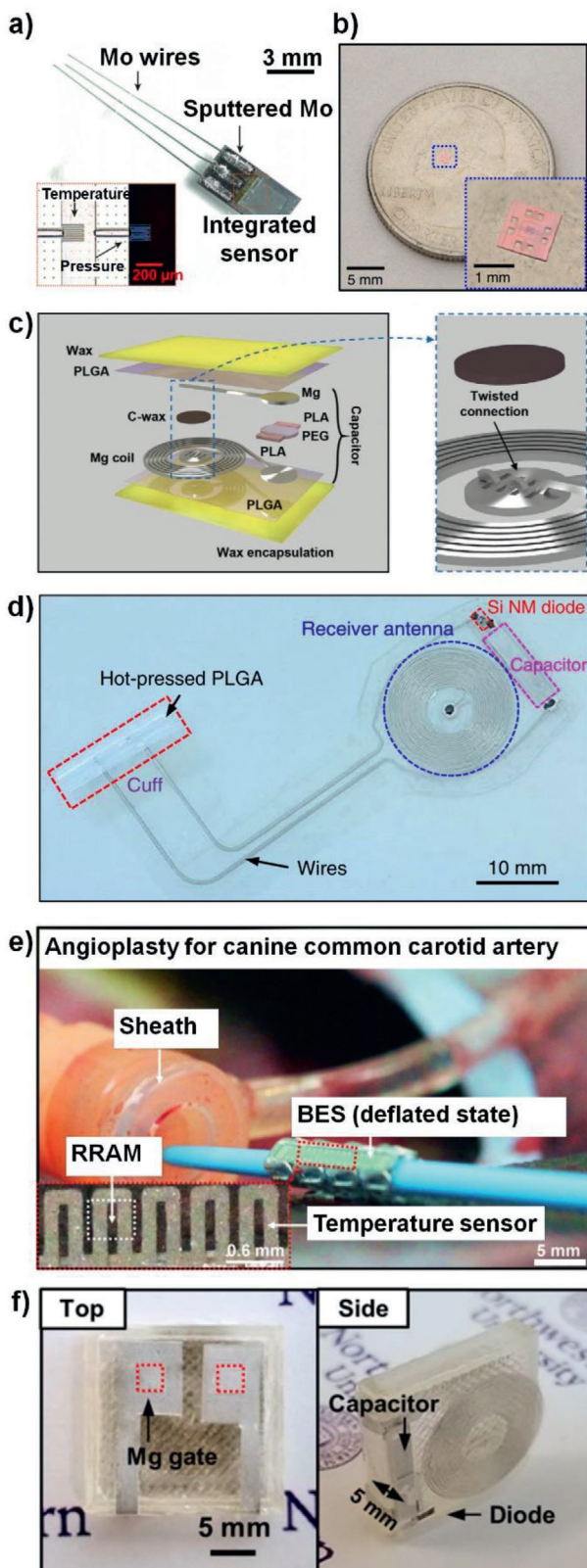


**Figure 7.** Bioresorbable metals in bioresorbable electronic devices designed for temporary diagnostic and/or therapeutic function. a) Image of bioresorbable pressure and temperature sensors with metal interconnects of Mg and Mo. The inset shows an optical micrograph of serpentine structures of Si-NMs as piezoresistive strain and temperature gauges. Adapted with permission.<sup>[28]</sup> Copyright 2016, Nature Publishing Group.

water and biological tissues is negligible. The shift in resonance frequency ( $\Delta f_0$ ) can be calculated according to:

$$\Delta f_0 = - \frac{\Delta C}{4\pi\sqrt{LC^3}} \quad (1)$$

where  $\Delta C$  is the change in capacitance,  $L$  and  $C$  are the inductance and the capacitance of the device, respectively. The diameter of the artery changes with pulsatile blood flow, thereby defining  $\Delta C$  and associated values of  $\Delta f_0$ . Pulse rates measured in this manner match those determined with a conventional Doppler ultrasound monitor. The use of thin, polymeric encapsulation layers (top layer; 10 μm thick poly(octamethylene maleate (anhydride) citrate) (POMaC), and bottom layer; 10 μm thick polyhydroxybutyrate/polyhydroxyvalerate (PHB/PHV)) lead to base capacitance values that drift over time shortly after implantation, leading to limitations in stable operating lifetimes.<sup>[122]</sup> Most components of the sensor, including the Mg wires and PGS film fully degrade after 12 weeks, leaving only the 10 μm thick PHB/PHV packaging layers.

Other types of LC oscillators allow measurements of regional internal body temperatures through changes in capacitance (Figure 7c).<sup>[121]</sup> Here, the capacitor uses the bioresorbable polymer polyethylene glycol (PEG) as the dielectric, a material that exhibits a strong temperature-dependent dielectric constant near body temperature (34–42 °C). This temperature dependence arises from the gradual “freezing” of rotational degrees of freedom of the PEG molecules below their melting point. Such freezing decreases the ability of PEG to screen electric fields by rotation of hydroxyl groups along the polymer backbone, thereby reducing the dielectric constant in this body temperature range. Shifts in the resonant frequency thus follow from mechanisms described in the previous paragraph, to allow wireless readout by inductive coupling. The device uses Mg electrodes for the capacitor and for the coil inductor (both 100 μm in thickness) patterned by laser cutting. The C-wax described previously serves as electrical interconnects. The stable operating period is 4 d after subcutaneous or intracranial implantation.

tine structures of Si-NMs as piezoresistive strain and temperature gauges. Adapted with permission.<sup>[28]</sup> Copyright 2016, Nature Publishing Group. b) Photograph of a pressure sensor resting on a quarter. The inset provides a magnified view. Adapted with permission.<sup>[119]</sup> Copyright 2018, The Author(s), under exclusive license to Springer Nature Limited. c) (left) Schematic illustration of the bioresorbable temperature sensor. (right) Magnified twisted connection image between the top electrode and the coil. The interconnection relies on a conductive paste, C-wax. Adapted with permission.<sup>[121]</sup> Copyright 2020, Wiley-VCH GmbH. d) Image of a bioreversible wireless electrical stimulator as a system to accelerate rates of neuroregeneration. Adapted with permission.<sup>[31]</sup> Copyright 2018, The Author(s), under exclusive license to Springer Nature America, Inc. e) Image of a bioreversible electronic stent (BES) installed on a balloon catheter during deployment into a canine common carotid artery. The inset shows the RRAM memory unit (white dotted box) and the temperature sensor (red dotted box). Adapted with permission.<sup>[27]</sup> Copyright 2015, American Chemical Society. f) Photograph of a wireless, bioresorbable device for programmed drug delivery. Adapted with permission.<sup>[49]</sup> Copyright 2020, The Authors, some rights reserved; exclusive license American Association for the Advancement of Science.

Bioresorbable electronic devices for therapeutic purposes are also possible. Initial demonstrations focus on wireless electrical stimulators to accelerate the rates of neuroregeneration for damaged peripheral nerves (Figure 7d).<sup>[31]</sup> Here, the device interfaces at a site along the nerve proximal to an injury and delivers DC electrical stimulation by wireless power transfer from an external coil. Thin films of Mg and bioresorbable conducting composites play important roles in the capacitors, inductors, electrical interconnects, antenna coils, and nerve interfaces. A Si NM diode rectifies the harvested AC power to yield a DC output to the nerve. C-wax forms electrical interfaces between the Mg antenna, the capacitor, and the diode. Ribbons of Mg (50 µm in thickness) embedded in PLGA define electrical connections between the wireless harvesting system and a cuff interface to the nerve, formed by a hot pressing process. In vivo studies use the devices as stimulators for up to 6 d after implantation, with clear benefits in accelerated rates of nerve regeneration and improved healing outcomes relative to control animals.

An interesting conceptual demonstration of a different type of therapeutic device involves a bioresorbable electronic stent that also combines sensing functionality (Figure 7e).<sup>[27]</sup> Here, a layer of poly(lactic acid) (PLA; 15 µm in thickness) encapsulates a stent formed in ZM21 Mg alloy (Mg-2Zn-1Mn; ≈200 µm in thickness, 27.4 mg) that also acts as an antenna for wireless communication. Integrated flow/temperature sensors use Mg (100 nm in thickness) and memory elements exploit a trilayer of Mg/MgO/Mg (60 nm/80 nm/60 nm). The PLA encapsulation layer includes ceria NPs to suppress inflammation. A capability for hyperthermia-based drug delivery uses gold nanorod core/mesoporous silica NP shells (AuNR@MS; diameters of ≈100 nm). Multilayer structures of PLA and MgO encapsulate the devices to slow the rates of degradation. In vivo and ex vivo animal experiments and studies in cell cultures demonstrate the basic functions.

An alternative class of drug delivery platform uses a wirelessly controlled, bioresorbable fluidic device with wirelessly programmable valves that seal underlying reservoirs filled with drugs (Figure 7f).<sup>[49]</sup> The mechanism for opening the valves relies on electrochemically triggered crevice corrosion of thin films of Mg (30 µm in thickness), using power harvested wirelessly by a sub-system similar to that for the nerve stimulators described previously. Here, a coil of Mg (50 µm in thickness, ≈100 µg) serves as an antenna, a trilayer of Mg/SiO<sub>2</sub>/Mg (30 µm/100 nm/30 µm) as a capacitor and a Si NM (320 nm in thickness) as the active part of an RF diode. Evaluations in cell cultures demonstrate the efficacy for treatment of cancerous tissues by release of doxorubicin using simple, single-reservoir devices. Combining separate antennas with distinct resonant frequencies 5.14, 9.92, and 14.78 MHz allows three independently programmed events to release insulin (0.9 IU diluted in 0.2 mL of PBS) at different time points. Another related system allows for directional and localized release of lidocaine (0.2%, ≈20 µL) on the sciatic nerve for local pain block. Here, a cuff structure of PLGA (4 mm × 8 mm; ≈20 µm in thickness) wraps the nerve and connects to three independent reservoirs. Studies with male Lewis rats illustrate possibilities for multiple, independently controlled release events for modulating blood glucose levels by timed delivery of insulin, and for blocking nerve function by timed delivery of lidocaine.

## 7. Conclusions and Perspectives

This paper highlights advances in bioresorbable metals through discussions of material options, biocompatibility aspects, and biomedical applications. Interest in this area follows mainly from the broad potential utility of these materials in medical systems, although there are additional opportunities for important uses in environmental monitoring, biological research and others. The choice of material depends strongly on the requirements of the application. **Table 1** summarizes key characteristics of bioresorbable metals featured in this article. Based on their favorable mechanical and corrosion properties, Mg, Zn, and Fe are attractive for bone fixtures, tissue and bone scaffolds, and stents. Uses in these areas are well studied and the materials science aspects, in many cases, are relatively mature. By comparison, electronic applications are more recent and they involve a complementary set of considerations. Metals explored for structural applications are of interest in this context, but others such as Mo and W, along with various composites with bioresorbable polymers, are also relevant. Methods in deposition and processing adapted from the semiconductor industry serve as the basis for forming these metals into electrodes, interconnects, antennas, and other necessary elements of the devices, where the thicknesses typically range from tens of microns to tens of nanometers. Interesting topics in thin film corrosion, morphology, surface chemistry, reaction-diffusion kinetics and others are critically important in this context. These phenomena can be qualitatively different from those studied in the past for structural applications of these same materials.

Prospects for research in this broader area of materials science are enhanced not only by these emerging areas of opportunity but also by continued commercial progress in passive bioresorbable devices, not only those based on metals, but also those that use polymers such as polycaprolactone (PCL), poly-L-lactic acid (PLLA), poly-D, L-lactic acid (PDLLA), and PLGA (see **Table 2**). As one example, MgYREZr-based bioabsorbable screws (MagnezixCS, Syntellix AG, Germany) show high efficacy in implants already deployed in many thousands of patients, also without introducing artifacts in magnetic resonance imaging (MRI) and computerized tomography (CT) scans.<sup>[125]</sup> Other bioresorbable devices have exhibited some initial promise, only to be followed by instances of isolated adverse health consequences. The implication for research in the healthcare materials science of these systems is that issues of biocompatibility and biological consequences of bioresorbable metals are complex and subtle, and therefore demand careful study. In general, minimizing the total mass load on the body may represent an important design consideration. In this sense, the minute amounts of materials necessary to address requirements bioresorbable thin-film electronics may represent an advantage.

In these contexts and others, many opportunities exist for research on bioresorbable metals and devices built with them. Expanding the range of alloys and structure geometries represents one important direction, where goals include controlled rates and modes of bioresorption and/or physiochemically stimuli-responsive behaviors. Materials strategies that allow for remotely controlled or triggered bioresorption are aspirational targets that could lead to unique modes of use, as well as enhanced safety profiles. Here and in other cases, composites that combine

**Table 1.** Summary of characteristics of bioresorbable metals.

Element	Pathophysiology <sup>[23]</sup>	Serum concentration [mmol L <sup>-1</sup> ] <sup>[24]</sup>	Recommended daily intake [mg] <sup>[24]</sup>	In vivo Toxicity (LD <sub>50</sub> ) obtained via oral supplement <sup>[124]</sup>	Corrosion rate of thin films in DI water [nm h <sup>-1</sup> ] <sup>[44]</sup>	Electrical degradation rate of thin films in DI water [μm h <sup>-1</sup> ] <sup>[44]</sup>	Applications
Mg	Activator of many enzymes; coregulator of protein synthesis and muscle contraction; stabilizer of DNA	0.7–1.0	280–350	5 000 mg kg <sup>-1</sup> (MgCl <sub>2</sub> )	≈70	0.3 ± 0.1	Structures, electrodes, interconnections
Zn	Trace element; appears in all enzyme classes; most Zn appears in muscle	12–18 × 10 <sup>-3</sup>	12–15	350 mg kg <sup>-1</sup> (ZnCl <sub>2</sub> )	≈7	0.07 ± 0.02	Structures, electrodes, interconnections
Fe	Component of several metalloproteins; be crucial in vital biochemical activities	13–31 × 10 <sup>-3</sup>	10–15	1300 mg kg <sup>-1</sup> (FeCl <sub>3</sub> )	–	<0.001	Structures, electrodes, interconnections
Mo	Trace element	62.5 × 10 <sup>-6</sup> –5.6 × 10 <sup>-3</sup>	25–75 × 10 <sup>-3</sup>	–	≈0.3	(1 ± 0.1) × 10 <sup>-3</sup>	Electrodes, interconnections
W	Nontoxic trace elements with un-known functions	31.5 × 10 <sup>-6</sup>	10 × 10 <sup>-3</sup>	–	≈0.3	(4 ± 1) × 10 <sup>-3</sup>	Electrodes, interconnections

**Table 2.** Summary of commercial biodegradable structures.

Commercial name	Manufacturer	Category	Major backbone material	Bioresorption time (months)	EU CE mark	FDA approval	Drug release
ABSORB GT1 <sup>[11]</sup> ART Pure <sup>[11]</sup>	Abbott	Scaffold	PLLA	24–36	Jan 2011	July 2016	Everolimus Drug-free
MERES 100 <sup>[11]</sup> Osteoplug/Osteomesh	Arterial Remodelling Technologies Meril Life Sciences Osteopore	Scaffold	PDLA PCL	12–24 24	May 2015	No	Sirolimus
Magmaris <sup>[11]</sup> IBS <sup>[11]</sup>	Biotronik	Stent	Mg	24	August 2019	No/2019 GMP inspection	–
MagnezixCS	Lifetech Scientific Syntelix	Stent Screw	Fe MgYREZ <sup>r</sup>	>12 12	June 2016 2013	No No	Sirolimus Sirolimus
MILAGROADVANCE	Depuy Synthes Mitek Sports Medicine	Screw	PLGA	36	2020 Breakthrough Device	2013 510(k) clearances	–

metals and polymers could create additional options in designs and applications. Most structural applications focus on high strength and on modulus values in the range of those of hard biomaterials like bone. By contrast, other applications, such as those in bioresorbable electronics, demand soft, compliant mechanics to allow for gentle interfaces to soft tissues. Bioresorbable conductors that combine metal nanostructures such as nanowires, nanoribbons, NMs, NPs and others with low modulus polymers or hydrogels can yield stretchable, flexible, foldable, and low resistance electrodes.<sup>[126,127]</sup> Other composite approaches exploit layered geometries where, for example, bioresorbable but insulating coatings serve as biofluid barriers to underlying bioresorbable metal structures to extend their functional lifetimes. These and other possibilities in multimaterial structures appear to be promising. In all cases, processes for fabricating the necessary composites and/or structures and for integrating them into functional devices are extremely important. Here, emerging methods in 3D printing, extrusion, micromachining and others could complement traditional techniques. The essential role of materials science, together with interdisciplinary content in mechanical engineering, biomedical engineering, manufacturing science and others, define a compelling area for research, further enhanced by its potential to significantly improve the care of patients.

## Acknowledgements

This work was supported by the Center for Bio-Integrated Electronics of the Querrey-Simpson Institute for Bioelectronics at Northwestern University. H.R. acknowledges support from the Basic Science Research Program (NRF-2019R1A6A3A12031359) through a National Research Foundation (NRF) of Korea Grant funded by the Ministry of Science and ICT. G.D.

## Conflict of Interest

The authors declare no conflict of interest.

## Keywords

biomedical implants, bioresorbable electronics, bioresorbable metals, bioresorbable structures, transient electronics

Received: December 21, 2020

Revised: January 29, 2021

Published online: February 15, 2021

- [1] Y. S. Choi, J. Koo, Y. J. Lee, G. Lee, R. Avila, H. Ying, J. Reeder, L. Hamitzer, K. Im, J. Kim, K. M. Lee, J. Cheng, Y. Huang, S. K. Kang, J. A. Rogers, *Adv. Funct. Mater.* **2020**, *30*, 2000941.
- [2] H. C. Tan, R. Ananthakrishna, *Singapore Med. J.* **2017**, *58*, 512.
- [3] G. D. Cha, D. Kang, J. Lee, D. H. Kim, *Adv. Healthcare Mater.* **2019**, *8*, e1801660.
- [4] H. Y. Ang, H. Bulluck, P. Wong, S. S. Venkatraman, Y. Huang, N. Foin, *Int. J. Cardiol.* **2017**, *228*, 931.
- [5] E. Charpentier, A. Barna, L. Guillevin, J. M. Juliard, *Arch. Cardiovasc. Dis.* **2015**, *108*, 385.
- [6] T. Kanno, S. Sukegawa, Y. Furuki, Y. Nariai, J. Sekine, *Jpn. Dent. Sci. Rev.* **2018**, *54*, 127.

- [7] L. Yang, M. Xu, X. Jin, J. Xu, J. Lu, C. Zhang, S. Li, L. Teng, *J. Cranio-Maxillofacial Surg.* **2014**, *42*, e176.
- [8] P. W. Serruys, H. M. Garcia-Garcia, Y. Onuma, *Eur. Heart J.* **2012**, *33*, 16.
- [9] Y. Choi, J. Koo, J. A. Rogers, *MRS Bull.* **2020**, *45*, 103.
- [10] G. Lee, Y. S. Choi, H.-J. Yoon, J. A. Rogers, *Matter* **2020**, *3*, 1031.
- [11] J. Wiebe, H. M. Nef, C. W. Hamm, *J. Am. Coll. Cardiol.* **2014**, *64*, 2541.
- [12] C. Li, C. Guo, V. Fitzpatrick, A. Ibrahim, M. J. Zwierstra, P. Hanna, A. Lechtig, A. Nazarian, S. J. Lin, D. L. Kaplan, *Nat. Rev. Mater.* **2019**, *5*, 61.
- [13] J. E. Moore, J. S. Soares, K. R. Rajagopal, *Cardiovasc. Eng. Technol.* **2010**, *1*, 52.
- [14] D. Zindani, K. Kumar, J. Paulo Davim, in *Mechanical Behaviour of Biomaterials* (Ed: J. P. Davim), Elsevier, Amsterdam, Netherlands **2019**, Ch. 4.
- [15] D. Zhao, F. Witte, F. Lu, J. Wang, J. Li, L. Qin, *Biomaterials* **2017**, *112*, 287.
- [16] F. Witte, *Acta Biomater.* **2010**, *6*, 1680.
- [17] E. Payr, *Arch. Klin. Chir.* **1900**, *62*, 67.
- [18] A. Lambotte, *Presse Med. Belge* **1909**, *17*, 321.
- [19] J. Verbrugge, *Presse Med.* **1934**, *23*, 460.
- [20] O. Maier, *Dtsch. Z. Chir.* **1940**, *253*, 552.
- [21] B. В. Троицкий, Д.Н. Цитрин, *Хирургия* **1948**, *8*, 41.
- [22] M. Peuster, P. Wohlsein, M. Brugmann, M. Ehlerding, K. Seidler, C. Fink, H. Brauer, A. Fischer, G. Hausdorf, *Heart* **2001**, *86*, 563.
- [23] F. Witte, J. Reifenrath, P. P. Müller, H. A. Crostack, J. Nellesen, F. W. Bach, D. Bormann, M. Rudert, *Materialwiss. Werkstofftech.* **2006**, *37*, 504.
- [24] D. H. Kim, Y. S. Kim, J. Amsden, B. Panilaitis, D. L. Kaplan, F. G. Omenetto, M. R. Zakin, J. A. Rogers, *Appl. Phys. Lett.* **2009**, *95*, 133701.
- [25] S.-W. Hwang, H. Tao, D.-H. Kim, H. Cheng, J.-K. Song, E. Rill, M. A. Brenckle, B. Panilaitis, S. M. Won, Y.-S. Kim, Y. M. Song, K. J. Yu, A. Ameen, R. Li, Y. Su, M. Yang, D. L. Kaplan, M. R. Zakin, M. J. Slepian, Y. Huang, F. G. Omenetto, J. A. Rogers, *Science* **2012**, *337*, 1640.
- [26] S. W. Hwang, C. H. Lee, H. Cheng, J. W. Jeong, S. K. Kang, J. H. Kim, J. Shin, J. Yang, Z. Liu, G. A. Ameer, Y. Huang, J. A. Rogers, *Nano Lett.* **2015**, *15*, 2801.
- [27] D. Son, J. Lee, D. J. Lee, R. Ghaffari, S. Yun, S. J. Kim, J. E. Lee, H. R. Cho, S. Yoon, S. Yang, S. Lee, S. Qiao, D. Ling, S. Shin, J.-K. Song, J. Kim, T. Kim, H. Lee, J. Kim, M. Soh, N. Lee, C. S. Hwang, S. Nam, N. Lu, T. Hyeon, S. H. Choi, D.-H. Kim, *ACS Nano* **2015**, *9*, 5937.
- [28] S. K. Kang, R. K. Murphy, S. W. Hwang, S. M. Lee, D. V. Harburg, N. A. Krueger, J. Shin, P. Gamble, H. Cheng, S. Yu, Z. Liu, J. G. McCall, M. Stephen, H. Ying, J. Kim, G. Park, R. C. Webb, C. H. Lee, S. Chung, D. S. Wie, A. D. Gujar, B. Vemulapalli, A. H. Kim, K. M. Lee, J. Cheng, Y. Huang, S. H. Lee, P. V. Braun, W. Z. Ray, J. A. Rogers, *Nature* **2016**, *530*, 71.
- [29] K. J. Yu, D. Kuzum, S. W. Hwang, B. H. Kim, H. Juul, N. H. Kim, S. M. Won, K. Chiang, M. Trumpis, A. G. Richardson, H. Cheng, H. Fang, M. Thomson, H. Bink, D. Talos, K. J. Seo, H. N. Lee, S. K. Kang, J. H. Kim, J. Y. Lee, Y. Huang, F. E. Jensen, M. A. Dichter, T. H. Lucas, J. Viventi, B. Litt, J. A. Rogers, *Nat. Mater.* **2016**, *15*, 782.
- [30] G. A. Salvatore, J. Sülzle, F. Dalla Valle, G. Cantarella, F. Robotti, P. Jokic, S. Knobelspies, A. Daus, L. Büthe, L. Petti, N. Kirchgessner, R. Hopf, M. Magno, G. Tröster, *Adv. Funct. Mater.* **2017**, *27*, 1702390.
- [31] J. Koo, M. R. MacEwan, S. K. Kang, S. M. Won, M. Stephen, P. Gamble, Z. Xie, Y. Yan, Y. Y. Chen, J. Shin, N. Birenbaum, S. Chung, S. B. Kim, J. Khalifeh, D. V. Harburg, K. Bear, M. Paskett, J. Kim, Z. S. Zohny, S. M. Lee, R. Zhang, K. Luo, B. Ji, A. Banks, H. M. Lee, Y. Huang, W. Z. Ray, J. A. Rogers, *Nat. Med.* **2018**, *24*, 1830.
- [32] D. Lu, T. L. Liu, J. K. Chang, D. Peng, Y. Zhang, J. Shin, T. Hang, W. Bai, Q. Yang, J. A. Rogers, *Adv. Mater.* **2019**, *31*, 1902739.

- [33] W. Bai, J. Shin, R. Fu, I. Kandela, D. Lu, X. Ni, Y. Park, Z. Liu, T. Hang, D. Wu, Y. Liu, C. R. Haney, I. Stepien, Q. Yang, J. Zhao, K. R. Nandoliya, H. Zhang, X. Sheng, L. Yin, K. MacRenaris, A. Brikha, F. Aird, M. Pezhouh, J. Hornick, W. Zhou, J. A. Rogers, *Nat. Biomed. Eng.* **2019**, *3*, 644.
- [34] J. K. Chang, M. A. B. Emon, C. S. Li, Q. Yang, H. P. Chang, Z. Yang, C. I. Wu, M. T. Saif, J. A. Rogers, *ACS Nano* **2018**, *12*, 9721.
- [35] R. Singh, M. J. Bathaei, E. Istif, L. Beker, *Adv. Healthcare Mater.* **2020**, *9*, e2000790.
- [36] J. L. Wang, J. K. Xu, C. Hopkins, D. H. Chow, L. Qin, *Adv. Sci.* **2020**, *7*, 1902443.
- [37] C. Hehrlein, B. Schorch, N. Kress, A. Arab, C. von Zur Muhlen, C. Bode, T. Epting, J. Haberstroh, L. Mey, H. Schwarzbach, R. Kinscherf, V. Stachniss, S. Schiestel, A. Kovacs, H. Fischer, E. Nennig, *PLoS One* **2019**, *14*, e0209111.
- [38] M. F. Ulum, A. K. Nasution, A. H. Yusop, A. Arafat, M. R. Kadir, V. Juniantito, D. Noviana, H. Hermawan, *J. Biomed. Mater. Res., Part B* **2015**, *103*, 1354.
- [39] K. K. Fu, Z. Wang, J. Dai, M. Carter, L. Hu, *Chem. Mater.* **2016**, *28*, 3527.
- [40] S. Chatterjee, M. Saxena, D. Padmanabhan, M. Jayachandra, H. J. Pandya, *Biosens. Bioelectron.* **2019**, *142*, 111489.
- [41] H.-S. Han, S. Loffredo, I. Jun, J. Edwards, Y.-C. Kim, H.-K. Seok, F. Witte, D. Mantovani, S. Glyn-Jones, *Mater. Today* **2019**, *23*, 57.
- [42] C. Chen, J. Chen, W. Wu, Y. Shi, L. Jin, L. Petrini, L. Shen, G. Yuan, W. Ding, J. Ge, E. R. Edelman, F. Migliavacca, *Biomaterials* **2019**, *221*, 119414.
- [43] N. T. Kirkland, N. Birbilis, M. P. Staiger, *Acta Biomater.* **2012**, *8*, 925.
- [44] L. Yin, H. Cheng, S. Mao, R. Haasch, Y. Liu, X. Xie, S.-W. Hwang, H. Jain, S.-K. Kang, Y. Su, R. Li, Y. Huang, J. A. Rogers, *Adv. Funct. Mater.* **2014**, *24*, 645.
- [45] A. Stefansson, *Environ. Sci. Technol.* **2007**, *41*, 6117.
- [46] W. A. Badawy, F. M. Al-Kharafi, *Electrochim. Acta* **1998**, *44*, 693.
- [47] E. Patrick, M. E. Orazem, J. C. Sanchez, T. Nishida, *J. Neurosci. Methods* **2011**, *198*, 158.
- [48] Y. F. Zheng, X. N. Gu, F. Witte, *Mater. Sci. Eng., R* **2014**, *77*, 1.
- [49] J. Koo, S. B. Kim, Y. S. Choi, Z. Xie, A. J. Bandodkar, J. Khalifeh, Y. Yan, H. Kim, M. K. Pezhouh, K. Doty, G. Lee, Y.-Y. Chen, S. M. Lee, D. D'Andrea, K. Jung, K. H. Lee, K. Li, S. Jo, H. Wang, J. H. Kim, J. Kim, S.-G. Choi, W. J. Jang, Y. S. Oh, I. Park, S. S. Kwak, J.-H. Park, D. Hong, X. Feng, C.-H. Lee, A. Banks, C. Leal, H. M. Lee, Y. Huang, C. K. Franz, W. Ray, M. MacEwan, S.-K. Kang, J. A. Rogers, *Sci. Adv.* **2020**, *6*, eabb1093.
- [50] ISO 10993–5:2009(E), *Biological Evaluation of Medical Devices – Part 5: Tests for in Vitro Cytotoxicity*, International Organization for Standardization, **2009**. <https://www.iso.org/standard/36406.html>
- [51] ISO 10993–3:2014(E), *Biological evaluation of medical devices—Part 3: Tests for genotoxicity, carcinogenicity and reproductive toxicity*, International Organization for Standardization, **2014**. <https://www.iso.org/standard/55614.html>
- [52] D. C. Swinney, in *Annual Reports in Medicinal Chemistry* (Ed: J. E. Macor), Elsevier, Amsterdam, Netherlands **2011**, Ch. 18.
- [53] M. Zhang, D. Aguilera, C. Das, H. Vasquez, P. Zage, V. Gopalakrishnan, J. Wolff, *Anticancer Res.* **2007**, *27*, 35.
- [54] J. W. Trevan, *Proc. R. Soc., Ser. B* **1927**, *101*, 483.
- [55] Y. Okazaki, S. Rao, S. Asao, T. Tateishi, *Mater. Trans., JIM* **1998**, *39*, 1070.
- [56] A. Yamamoto, R. Honma, M. Sumita, *J. Biomed. Mater. Res.* **1998**, *39*, 331.
- [57] N. J. Hallab, C. Vermees, C. Messina, K. A. Roebuck, T. T. Glant, J. J. Jacobs, *J. Biomed. Mater. Res.* **2002**, *60*, 420.
- [58] M. Peuster, C. Fink, C. v. Schnakenburg, *Biomaterials* **2003**, *24*, 4057.
- [59] D. Bian, J. Deng, N. Li, X. Chu, Y. Liu, W. Li, H. Cai, P. Xiu, Y. Zhang, Z. Guan, Y. Zheng, Y. Kou, B. Jiang, R. Chen, *ACS Appl. Mater. Interfaces* **2018**, *10*, 4394.
- [60] M. J. Akhtar, M. Ahmed, H. A. Alhadlaq, A. Alshamsan, M. A. Khan, S. A. Alrokayan, *J. Colloid Interface Sci.* **2015**, *457*, 370.
- [61] S. Zhu, N. Huang, L. Xu, Y. Zhang, H. Liu, H. Sun, Y. Leng, *Mater. Sci. Eng. C* **2009**, *29*, 1589.
- [62] E. R. Shearier, P. K. Bowen, W. He, A. Drelich, J. Drelich, J. Goldman, F. Zhao, *ACS Biomater. Sci. Eng.* **2016**, *2*, 634.
- [63] K. A. Jansen, D. M. Donato, H. E. Balcioglu, T. Schmidt, E. H. Danen, G. H. Koenderink, *Biochim. Biophys. Acta* **2015**, *1853*, 3043.
- [64] W. Wang, G. Jia, Q. Wang, H. Huang, X. Li, H. Zeng, W. Ding, F. Witte, C. Zhang, W. Jia, G. Yuan, *Mater. Des.* **2020**, *189*, 108514.
- [65] S.-W. Hwang, D.-H. Kim, H. Tao, T.-i. Kim, S. Kim, K. J. Yu, B. Panilaitis, J.-W. Jeong, J.-K. Song, F. G. Omenetto, J. A. Rogers, *Adv. Funct. Mater.* **2013**, *23*, 4087.
- [66] W. Chao, Q. Hong, H. Xiao-ying, R. Ying-mao, T. Yi, C. Yan, X. Xin-lin, X. Liang, T. Yue, G. Run-lin, *Chin. Med. J.* **2013**, *126*, 4752.
- [67] A. Kafri, S. Ovadia, G. Yosafovich-Doitch, E. Aghion, *J. Mater. Sci.: Mater. Med.* **2018**, *29*, 94.
- [68] R. Erbel, C. Di Mario, J. Bartunek, J. Bonnier, B. de Bruyne, F. R. Eberli, P. Erne, M. Haude, B. Heublein, M. Horrigan, C. Ilsley, D. Böse, J. Koolen, T. F. Lüscher, N. Weissman, R. Waksman, *Lancet* **2007**, *369*, 1869.
- [69] S. M. Won, J. Koo, K. E. Crawford, A. D. Mickle, Y. Xue, S. Min, L. A. McIlvried, Y. Yan, S. B. Kim, S. M. Lee, B. H. Kim, H. Jang, M. R. MacEwan, Y. Huang, R. W. Gereau, J. A. Rogers, *Adv. Funct. Mater.* **2018**, *28*, 1801819.
- [70] R. C. Thomson, M. C. Wake, M. J. Yaszemski, A. G. Mikosa, in *Biopolymers II. Advances in Polymer Science*, Vol 122. Springer, Berlin, Heidelberg **2005**.
- [71] A. U. Daniels, M. K. O. Chang, K. P. Andriano, J. Heller, *J. Appl. Biomater.* **1990**, *1*, 57.
- [72] G. S. Kwond, D. Y. Furgeson, in *Biomedical Polymers* (Ed: M. Jenkins), Elsevier, Amsterdam, Netherlands **2007**, Ch. 4.
- [73] J. W. Lee, H. S. Han, K. J. Han, J. Park, H. Jeon, M. R. Ok, H. K. Seok, J. P. Ahn, K. E. Lee, D. H. Lee, S. J. Yang, S. Y. Cho, P. R. Cha, H. Kwon, T. H. Nam, J. H. Han, H. J. Rho, K. S. Lee, Y. C. Kim, D. Mantovani, *Proc. Natl. Acad. Sci. USA* **2016**, *113*, 716.
- [74] Y. Chen, Z. Xu, C. Smith, J. Sankar, *Acta Biomater.* **2014**, *10*, 4561.
- [75] C. K. Seal, K. Vince, M. A. Hodgson, *IOP Conf. Ser.: Mater. Sci. Eng.* **2009**, *4*, 012011.
- [76] M. P. Staiger, A. M. Pietak, J. Huadmai, G. Dias, *Biomaterials* **2006**, *27*, 1728.
- [77] Z.-M. Huang, K. Fujihara, *Compos. Sci. Technol.* **2005**, *65*, 73.
- [78] H. K. Schwyzer, J. Cordey, S. Brun, P. Matter, S. M. Perren, *Biomechanics: Current Interdisciplinary Research*, Springer, Dordrecht, Netherlands **1985**.
- [79] S. Hidaka, R. B. Gustilo, *J. Bone Jt. Surg.* **1984**, *66*, 1241.
- [80] P. A. Deluca, R. W. Lindsey, p. A. Ruwe, *J. Bone Jt. Surg.* **1988**, *70*, 1372.
- [81] S. A. Borgave, S. S. Awati, R. M. Deshmukh, *IOSR-JMCE* **2018**, *8*, 45.
- [82] M. Moravej, D. Mantovani, *Int. J. Mol. Sci.* **2011**, *12*, 4250.
- [83] R. Hou, J. Victoria-Hernandez, P. Jiang, R. Willumeit-Romer, B. Luthringer-Feyerabend, S. Yi, D. Letzig, F. Feyerabend, *Acta Biomater.* **2019**, *97*, 608.
- [84] M. B. Kannan, W. Dietzel, R. K. S. Raman, P. Lyon, *Scr. Mater.* **2007**, *57*, 579.
- [85] M. Q. Cheng, T. Wahafu, G. F. Jiang, W. Liu, Y. Q. Qiao, X. C. Peng, T. Cheng, X. L. Zhang, G. He, X. Y. Liu, *Sci. Rep.* **2016**, *6*, 24134.
- [86] Y. Q. Zhu, K. Yang, L. Edmonds, L. M. Wei, R. Zheng, R. Y. Cheng, W. G. Cui, Y. S. Cheng, *Ther. Adv. Gastroenterol.* **2017**, *10*, 11.

- [87] J. Reifenrath, N. Angrisani, N. Erdmann, A. Lucas, H. Waizy, J. M. Seitz, A. Bondarenko, A. Meyer-Lindenberg, *Biomed. Mater.* **2013**, *8*, 045012.
- [88] L. Wolters, N. Angrisani, J. Seitz, P. Helmecke, A. Weizbauer, J. Reifenrath, *Biomed. Technol.* **2013**, *58*, 4059.
- [89] N. Erdmann, N. Angrisani, J. Reifenrath, A. Lucas, F. Thorey, D. Bornmann, A. Meyer-Lindenberg, *Acta Biomater.* **2011**, *7*, 1421.
- [90] H. Windhagen, K. Radtke, A. Weizbauer, J. Diekmann, Y. Noll, U. Kreimeyer, R. Schavan, C. Stukenborg-Colsman, H. Waizy, *Biomed. Eng. Online* **2013**, *12*, 62.
- [91] H. Hermawan, *Prog. Biomater.* **2018**, *7*, 93.
- [92] C. H. Chang, F. H. Lin, T. F. Kuo, H. C. Liu, *Biomed. Eng.: Appl. Basis Commun.* **2005**, *17*, 61.
- [93] M. V. Risbud, M. Sittinger, *Trends Biotechnol.* **2002**, *20*, 351.
- [94] A. H. Yusop, A. A. Bakir, N. A. Shaharom, M. R. Abdul Kadir, H. Hermawan, *Int. J. Biomater.* **2012**, *2012*, 641430.
- [95] F. J. O'Brien, *Mater. Today* **2011**, *14*, 88.
- [96] J. Fu, Y. Su, Y. X. Qin, Y. Zheng, Y. Wang, D. Zhu, *Biomaterials* **2020**, *230*, 119641.
- [97] Y. Su, I. Cockerill, Y. Wang, Y. X. Qin, L. Chang, Y. Zheng, D. Zhu, *Trends Biotechnol.* **2019**, *37*, 428.
- [98] P. K. Bowen, J. Drelich, J. Goldman, *Adv. Mater.* **2013**, *25*, 2577.
- [99] Z. Khurshid, M. S. Zafar, S. Hussain, A. Fareed, S. Yousaf, F. Sefat, in *Handbook of Ionic Substituted Hydroxyapatites* (Ed: A. S. Khan, A. A. Chaudhry), Elsevier, Amsterdam, Netherlands **2020**, Ch. 10.
- [100] J. Moore, G. Zouridakis, *Biomedical Technology and Devices Handbook*, CRC Press LLC, Boca Raton, FL, USA **2004**.
- [101] P. Sharma, R. Kozarek, the Practice Parameters Committee of American College of Gastroenterology, *Am. J. Gastroenterol.* **2010**, *105*, 258.
- [102] J. J. Bergman, L. Burgemeister, M. J. Bruno, E. A. Rauws, D. J. Gouma, G. N. Tytgat, K. Huibregtse, *Gastrointest. Endosc.* **2001**, *54*, 154.
- [103] B. S. Kapoor, B. May, N. Panu, K. Kowalik, D. W. Hunter, *J. Vasc. Intervention. Radiol.* **2007**, *18*, 629.
- [104] J. Y. Lock, E. Wyatt, S. Upadhyayula, A. Whall, V. Nunez, V. I. Vullev, H. Liu, *J. Biomed. Mater. Res., Part A* **2014**, *102*, 781.
- [105] J. E. Sousa, P. W. Serruys, M. A. Costa, *Circulation* **2003**, *107*, 2274.
- [106] S. Saito, *Catheter. Cardiovasc. Interventions* **2005**, *66*, 595.
- [107] P. Erne, M. Schier, T. J. Resink, *Cardiovasc. Interventions Radiol.* **2006**, *29*, 11.
- [108] M. Peuster, P. Wohlsein, M. Brügmann, M. Ehlerding, K. Seidler, C. Fink, H. Brauer, A. Fischer, G. Hausdorf, *Heart* **2001**, *86*, 563.
- [109] A. Colombo, E. Karvouni, *Circulation* **2000**, *102*, 371.
- [110] R. Waksman, R. Pakala, R. Baffour, R. Seabron, D. Hellinga, F. O. Tio, *J. Interventions Cardiol.* **2008**, *21*, 15.
- [111] B. Forrestal, B. C. Case, C. Yerasi, A. Musallam, C. Chezar-Azerrad, R. Waksman, *Rambam Maimonides Med. J.* **2020**, *11*, e0016.
- [112] J. K. Chang, H. Fang, C. A. Bower, E. Song, X. Yu, J. A. Rogers, *Proc. Natl. Acad. Sci. USA* **2017**, *114*, E5522.
- [113] S.-K. Kang, S.-W. Hwang, H. Cheng, S. Yu, B. H. Kim, J.-H. Kim, Y. Huang, J. A. Rogers, *Adv. Funct. Mater.* **2014**, *24*, 4427.
- [114] Q. Yang, S. Lee, Y. Xue, Y. Yan, T. L. Liu, S. K. Kang, Y. J. Lee, S. H. Lee, M. H. Seo, D. Lu, J. Koo, M. R. MacEwan, R. T. Yin, W. Z. Ray, Y. Huang, J. A. Rogers, *Adv. Funct. Mater.* **2020**, *30*, 1910718.
- [115] Y. K. Lee, J. Kim, Y. Kim, J. W. Kwak, Y. Yoon, J. A. Rogers, *Adv. Mater.* **2017**, *29*, 1702665.
- [116] S. Lee, J. Koo, S.-K. Kang, G. Park, Y. J. Lee, Y.-Y. Chen, S. A. Lim, K.-M. Lee, J. A. Rogers, *Mater. Today* **2018**, *21*, 207.
- [117] S. M. Won, J. Koo, K. E. Crawford, A. D. Mickle, Y. Xue, S. Min, L. A. McIlvried, Y. Yan, S. B. Kim, S. M. Lee, B. H. Kim, H. Jang, M. R. MacEwan, Y. Huang, R. W. Gereau IV, J. A. Rogers, *Adv. Funct. Mater.* **2018**, *28*, 1801819.
- [118] R. W. Bartlett, *J. Electrochem. Soc.* **1965**, *112*, 744.
- [119] J. Shin, Y. Yan, W. Bai, Y. Xue, P. Gamble, L. Tian, I. Kandela, C. R. Haney, W. Spees, Y. Lee, M. Choi, J. Ko, H. Ryu, J. K. Chang, M. Pezhouh, S. K. Kang, S. M. Won, K. J. Yu, J. Zhao, Y. K. Lee, M. R. MacEwan, S. K. Song, Y. Huang, W. Z. Ray, J. A. Rogers, *Nat. Biomed. Eng.* **2019**, *3*, 37.
- [120] C. M. Boutry, L. Beker, Y. Kaizawa, C. Vassos, H. Tran, A. C. Hinckley, R. Pfattner, S. Niu, J. Li, J. Claverie, Z. Wang, J. Chang, P. M. Fox, Z. Bao, *Nat. Biomed. Eng.* **2019**, *3*, 47.
- [121] D. Lu, Y. Yan, R. Avila, I. Kandela, I. Stepien, M. H. Seo, W. Bai, Q. Yang, C. Li, C. R. Haney, E. A. Waters, M. R. MacEwan, Y. Huang, W. Z. Ray, J. A. Rogers, *Adv. Healthcare Mater.* **2020**, *9*, e2000942.
- [122] M. A. Fonseca, M. G. Allen, J. Kroh, J. White, presented at *Proc. 12th Solid-State Sensors, Actuators and Microsystems Workshop*, Hilton Head Island, SC, June **2006**.
- [123] G. Katarivas Levy, J. Goldman, E. Aghion, *Metals* **2017**, *7*, 402.
- [124] Y. Liu, Y. Zheng, X. H. Chen, J. A. Yang, H. Pan, D. Chen, L. Wang, J. Zhang, D. Zhu, S. Wu, K. W. K. Yeung, R. C. Zeng, Y. Han, S. Guan, *Adv. Funct. Mater.* **2019**, *29*, 1805402.
- [125] J.-M. Seitz, A. Lucas, M. Kirschner, *JOM* **2016**, *68*, 1177.
- [126] L. Hu, H. S. Kim, J.-Y. Lee, P. Peumans, Y. Cui, *ACS Nano* **2010**, *4*, 2955.
- [127] C. Hwang, W. J. Song, J. G. Han, S. Bae, G. Song, N. S. Choi, S. Park, H. K. Song, *Adv. Mater.* **2018**, *30*, 1705445.



**Hanjun Ryu** obtained his B.S. degree in advanced materials science and engineering from the Sungkyunkwan University, Republic of Korea in 2014. From Sungkyunkwan University, he received his Ph.D. under the supervision of Prof. Sang-Woo Kim in materials science and engineering in 2019. Currently, he is a postdoctoral research fellow at the Querrey-Simpson Institute for Bioelectronics, Center for Bio-integrated Electronics (CBIE) at Northwestern University in the United States. His research interests are bioresorbable electrical stimulators/sensors for chronic wound healing, and 3D multifunctional mesoscale frameworks for organoids monitoring, and nanogenerators.



**Min-Ho Seo** received his B.S. degree in the Department of Nanomechatronics Engineering from Pusan National University (PNU) in 2011, and received his M.S. and Ph.D. degrees in the School of Electrical Engineering from the Korea Advanced Institute of Science and Technology (KAIST) in 2013 and 2018, respectively. From 2018 to 2019, he was a postdoctoral research fellow at the Information and Electronics Research Institute at KAIST. From 2019 to 2020, he was with the Center for Bio-integrated Electronics (CBIE) at Northwestern University in the United States as a postdoctoral research fellow. Since 2020, he has been with the School of Biomedical Convergence Engineering, PNU as an assistant professor. His research interests include nano/microelectromechanical systems (N/MEMS) and biomedical electronics.



**John A. Rogers** obtained his B.A. and B.S. degrees in chemistry and physics from the University of Texas, Austin, in 1989. From MIT, he received S.M. degrees in physics and chemistry in 1992 and a Ph.D. in physical chemistry in 1995. After five years at Bell Laboratories, he spent 13 years on the faculty at the University of Illinois Urbana-Champaign. In 2016, he joined Northwestern University as the Louis Simpson and Kimberly Querrey Professor of materials science and engineering, biomedical engineering and medicine, with affiliated appointments in mechanical engineering, electrical and computer engineering, and chemistry. Prof. Rogers also serves as Director of the Querrey-Simpson Institute for Bioelectronics.